

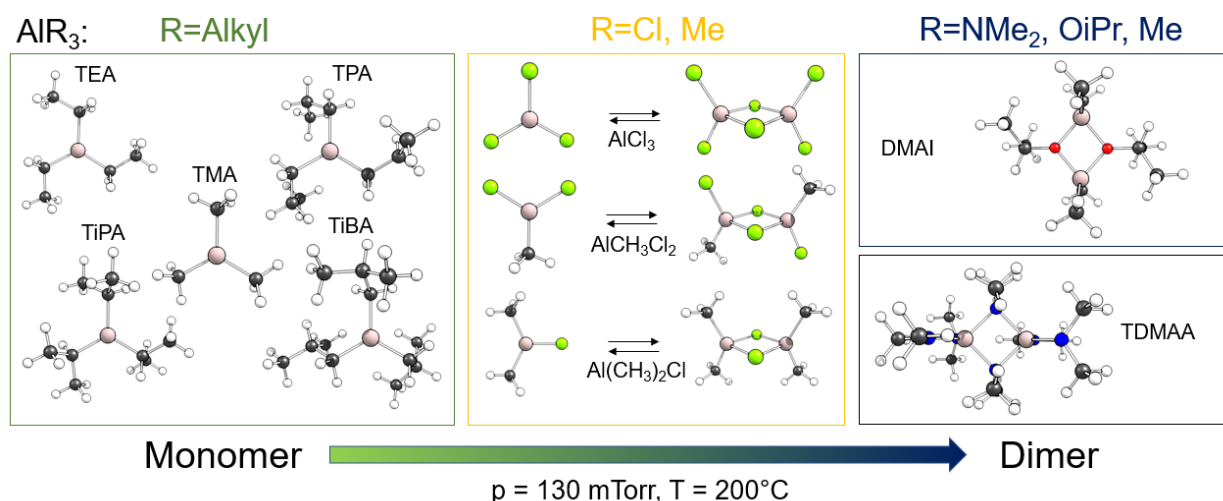
Accurately computed dimerization fraction of ALD precursors and their impact on surface reactivity in area-selective atomic layer deposition

Patrick Maue[†], Émilie Chantraine[†], Fabian Pieck[†], Ralf Tonner-Zech^{†,*}

[†]Patrick Maue, Emilie Chantraine, Dr. Fabian Pieck, Prof. Dr. Ralf Tonner-Zech
Fakultät für Chemie und Mineralogie, Wilhelm-Ostwald-Institut für Physikalische und
Theoretische Chemie, Universität Leipzig, Linnéstr. 2, 04103 Leipzig, Germany
e-mail: ralf.tonner@uni-leipzig.de
ORCID: Ralf Tonner-Zech 0000-0002-6759-8559, Fabian Pieck 0000-0001-6912-2725, Emilie
Chantraine 0009-0000-7086-0901

Abstract

The Lewis acidic nature of aluminum atoms in common precursors for the atomic layer deposition (ALD) of Al_2O_3 can lead to dimerization. This study investigates whether these compounds predominantly exist as monomers or dimers under ALD conditions. Understanding dimerization is crucial for discussing precursor reactivities and other properties, especially in the context of area-selective ALD (AS-ALD). We employed a theoretical approach, incorporating conformer search, density functional theory, and coupled cluster calculations, to determine the dissociated dimer fraction for a range of precursors under typical ALD pressures and temperatures. The precursors studied include aluminum alkyls, chlorinated aluminum alkyls, dimethylaluminumisopropoxide (DMAI), and trisdimethylamidoaluminum (TDMAA). Our findings indicate that aluminum alkyls are completely dissociated over the whole parameter range, while DMAI and TDMAA form stable dimers. Chlorinated precursors were found to exist in both monomeric and dimeric forms depending on temperature and pressure.



Keywords

AS-ALD, dimerization, aluminum, precursors, coupled cluster, density functional theory

1. Introduction

Atomic layer deposition (ALD) is a technique for the deposition of thin-film structures based on sequential precursor pulses to a substrate surface where they react and form the desired material.^{1–3} Applications of ALD include catalysts⁴, energy applications like fuel cells⁵, nanotechnology⁶ and semiconductor manufacturing^{1,2}. A vital parameter in ALD processes is the choice of precursor molecules.^{7,8} It has an influence on the deposition in many ways like differences in growth rates⁹, temperature and pressure at which ALD processes can be performed,¹⁰ the quality of the deposited material or the adsorption behavior¹¹.

Recently the area-selective variant of ALD (AS-ALD) gained strong popularity.³ Here, a material is controllably grown on one surface (the growth surface) while no deposition takes place on a second surface (the non-growth surface).¹² A major challenge of AS-ALD is the loss of selectivity after a certain number of cycles.^{3,13} Experiments have shown that the number of selective deposition steps before growth initiates on the non-growth area often depends on the precursor molecule that is applied in the process.^{14–16} This shows that the underlying precursor chemistry has an essential impact on the AS-ALD process. In case of the selective deposition of Al₂O₃, for example, a higher number of selective deposition steps was possible with dimethylaluminumisopropoxide (DMAI) compared to the most often used precursor trimethylaluminum (TMA).¹⁵ In the same way, triethylaluminum (TEA) outperformed TMA and a set of alkyl aluminumchlorides in terms of achieved selectivity.^{14,16} While selectivity in AS-ALD thus obviously depends on the choice of the precursor, the underlying reactivity is not yet fully revealed for many processes. Consequently, a better understanding of precursor chemistry is desirable to improve selectivity in current processes and to develop new AS-ALD processes.

The precursor chemistry is defined by the precursor size, its chemical reactivity and physical properties like volatility and thermal stability. The chemical reactivity in AS-ALD, for example, can be determined by the accessibility to and reactivity with reactive surface sites on non-growth areas, where effects of steric blocking¹⁷ and therefore the size of precursors matter. For this reason, one crucial question is whether a precursor is present as monomer or dimer under experimental ALD conditions (see Fig. 1). Most ALD precursors are Lewis-acids and thus form homomolecular dimers with the interdimer bond strength depending on their Lewis acidity and steric crowding.

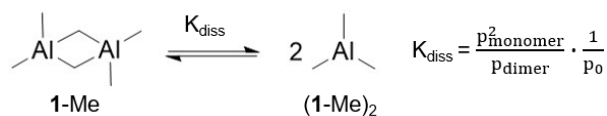


Figure 1. Dimerization reaction of Al precursors shown at the example of TMA with the equilibrium constant K_{diss} for the dissociation defined via the partial pressures p_{monomer} and p_{dimer} and standard pressure p_0 .

Dimers have bigger effective sizes and are less reactive than monomeric compounds.¹⁴ Both effects can crucially influence the selectivity in AS-ALD. The effect of dimerization has been recently investigated for Ga-precursors in the context of Chemical Vapor Deposition of GaN.¹⁸

For Al-based precursors, the question of dimerization has been discussed in the past. It is known that compounds commonly used as Al-precursors such as aluminum alkyls or alkyl aluminumchlorides^{2,9,19–22} as well as DMAI^{15,23} can dimerize^{14,19–23}. To estimate the monomer to dimer ratio, dimerization enthalpies or energies have been determined either theoretically or experimentally.^{14,20,21,24–26} However, the published values differ quite strongly: Hiraoka and Mashika²⁶ for example calculated a dissociation energy of $18 \text{ kJ}\cdot\text{mol}^{-1}$ for TMA based on Hartree-Fock (HF) and Møller-Plesset perturbation theory (MP2), whereas Oh et al.¹⁴ obtained a value of $77 \text{ kJ}\cdot\text{mol}^{-1}$ based on density functional theory (DFT) calculations. One reason for the deviations is the use of computational methods with limited accuracy like density functional theory (DFT) combined with moderately sized basis sets, which lead to considerable basis set superposition errors especially for association reactions.^{27,28}

A further problem of calculated enthalpies or Gibbs energies (ΔG) is that they are computed at pressures and temperatures that are not common for ALD applications. Often standard conditions of $T = 25^\circ\text{C}$ and $p = 1 \text{ bar}$ or 1 atm are used which are the default settings in common quantum chemistry software packages. However, ALD processes are usually performed at considerably higher temperatures and lower pressures (typical values are $T = 100\text{--}300^\circ\text{C}$ ³ and $p < 10^{-2} \text{ bar}$ ^{14,15,29,30}) causing strong changes in computed ΔG_{diss} values. However, an accurate determination of ΔG_{diss} is important because of its exponential relationship³¹ to the dissociation rate constant K_{diss} and thereby monomer to dimer ratio. Therefore, common errors of DFT calculations of $10 \text{ kJ}\cdot\text{mol}^{-1}$ already change the rate constant by one order of magnitude (see SI eq. (S1) and (S2)). Nevertheless, Marques et al. showed that DFT can often be used to predict

equilibrium compositions. For temperature dependent equilibrium compositions, however only a qualitative correct behavior has been predicted.³²

We thus set out to obtain accurate results by using highly accurate wavefunction based methods (CCSD(T), the so-called “gold standard”) together with a complete basis set (CBS) extrapolation scheme and several other methodological measures to derive accurate dimerization energies under typical ALD conditions. We use a set of contemporary Al precursors for ALD spanning a broad range of Lewis acidity and steric crowding (Fig. 2). Apart from the compound classes mentioned above, also trisdimethylamidoaluminum (TDMAA) can be applied as an ALD precursor^{33,17} and has been included in our set of precursors. The alkyl-aluminum compounds in this study include not only molecules with linear alkyl chains but also the molecules with branched chains, triisopropylaluminum (TiPA) and triisobutylaluminum (TiBA). The latter is an extensively studied precursor for the deposition of alumina films, and has been discussed before in the context of chemical vapor deposition.³⁴ We arrive at reliable dimerization fractions for these precursors. This will help to interpret ALD experiments as well as to choose ALD conditions to target a certain precursor state and can be crucial in AS-ALD where the dimerization can lead to increased selectivity. We show the impact of monomeric vs. dimeric precursor exemplarily for a case study of surface adsorption on clean and SMI-covered SiO₂.

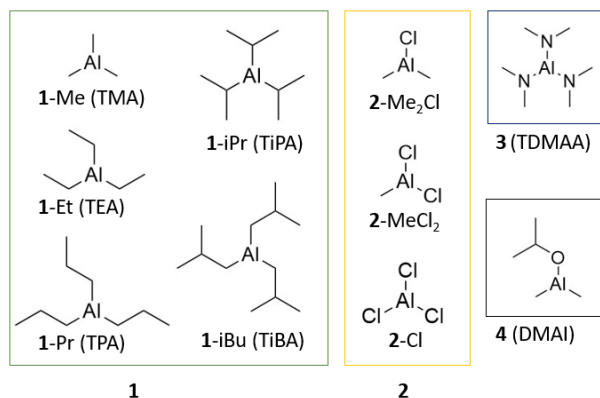


Figure 2. Set of aluminum precursors investigated in this study grouped in substance classes 1-4. Abbreviations used in the ALD literature are shown in brackets where available.

2. Computational details

2.1 Molecular calculations

2.1.1 Structural optimizations

Calculations of the monomers and dimers for the thermochemical properties were done with ORCA 5.0.3³⁵⁻⁴². Conformers were sampled with CREST^{43,44} using standard settings which include iMTD-GC workflow and GFN2-xTB. The three conformers lowest in energy were selected and reoptimized with B3LYP-D3. The conformer with the lowest Gibbs-free energy at 200°C and $1.73 \cdot 10^{-4}$ bar (130 mTorr), a realistic set of conditions for ALD processes,¹⁴ was then chosen for any further property calculations. No ensemble averages with multiple conformers were used in the calculation of energies and enthalpies. The effect which Boltzmann averaging can have on the dimerization energies and why it has been neglected in this study is discussed in 2.1 in the SI. For all calculations with density functional theory (DFT), the B3LYP⁴⁵⁻⁴⁷ exchange-correlation functional with DFT-D3 dispersion correction and a Becke-Johnson-type damping function (BJ) was applied.^{38,39} This combination showed the best agreement to CCSD(T) calculations in our benchmark study (see Tab. S2). A def2-TZVPP⁴⁸ basis set together with the corresponding auxiliary basis set for the RI approximation⁴⁹ was applied. The densest Becke-Integration Grid⁵⁰ “defgrid3” was used in all DFT calculations. To obtain the thermodynamic correction terms and ensure that the obtained geometries correspond to minimum structures, frequency calculations⁴¹ were performed. In all calculations, a convergence criterium for the self-consistent field (SCF) cycles of 10^{-8} E_h for the change in energy was used. For optimizations, ORCA uses several criteria based on the change in energy (10^{-6} E_h), the current gradient (root mean square: $3 \cdot 10^{-5}$ E_h·bohr⁻¹, largest value: 10^{-4} E_h·bohr⁻¹), as well as the step size of the optimization step (root mean square: $6 \cdot 10^{-4}$ bohr, largest value: 10^{-3} bohr). If imaginary frequencies were observed, the convergence criteria for optimizations were tightened to $2 \cdot 10^{-7}$ E_h, $8 \cdot 10^{-6}$ E_h·bohr⁻¹, $3 \cdot 10^{-5}$ E_h·bohr⁻¹, 10^{-4} bohr, and $2 \cdot 10^{-4}$ bohr, respectively. For difficult cases, structures were distorted along imaginary modes followed by structural optimizations until no imaginary modes were observed. The final electronic energy of each structure was obtained with a DLPNO-CCSD(T)^{42,51} single point calculation (in the following stated as CCSD(T)) including a complete basis set (CBS) extrapolation⁵² as implemented in ORCA. Here, the convergence of the HF energy to the basis set limit is extrapolated as:

$$E_{SCF}^{(X)} = E_{SCF}^{(\infty)} + A \cdot e^{-\alpha\sqrt{X}} \quad (1)$$

$E_{SCF}^{(X)}$ is the SCF energy of a basis set cc-pVXZ, with X=2 meaning a double zeta, X=3 triple zeta basis, etc. $E_{SCF}^{(\infty)}$ is the basis set limit SCF energy, α a basis set specific constant and A is the constant to be determined in the procedure.

The correlation energy contribution is extrapolated with $\beta=2.4$ as:

$$E_{corr}^{(\infty)} = \frac{X^\beta E_{corr}^{(X)} - Y^\beta E_{corr}^{(Y)}}{X^\beta - Y^\beta}. \quad (2)$$

We used X=3 and Y=4, thus the cc-pVTZ and cc-pVQZ^{49,53} basis sets. With these basis sets the value for α is 5.46. Furthermore, for all DLPNO computations, default thresholds were used after testing (see Tab. S3 for a discussion of this choice).

Gibbs free energies were calculated by adding thermodynamic correction terms obtained at B3LYP-D3 level of theory to CCSD(T) single point energies:

$$G = E(CCSD(T)) + G_{correction}(B3LYP - D3) \quad (3)$$

Here, all thermodynamic corrections were calculated via statistical thermodynamic approaches in double harmonic approximation with T= -50 - 400 °C in steps of 50 °C and p = 1.103·10⁻⁶ bar (10⁻⁶ atm, 0.76 mTorr) to 1.103 bar (1 atm, 7.6·10⁵ mTorr) in steps of one order of magnitude.

A detailed discussion of the conformer search (see Tab. S1 and S4), the effect of density functionals (see Tab. S2) and basis sets (see Tab. S5) can be found in the supporting information. The effect of the basis set superposition error (BSSE) has been tested by the application of counterpoise (CP) correction (see Tab. S6) and can lead to errors of up to 4.2 kJ·mol⁻¹. However, the application of a complete basis set (CBS) extrapolation for CCSD(T) calculations removes the problem of the BSSE. An overview of possible error sources and their estimated error is shown in Tab. S7.

2.1.2 Thermochemistry

With the inner energy U, p and V for pressure and volume, the enthalpy H is defined as³¹:

$$H = U + p \cdot V. \quad (4)$$

The Gibbs energy G of a reaction at temperature T is related to the enthalpy H and entropy S by³¹:

$$G = H - T \cdot S. \quad (5)$$

Free enthalpies of dissociation ΔG_{diss} were calculated as the difference between monomers and dimers:

$$\Delta G_{diss} = 2 \cdot G_{monomer} - G_{dimer}. \quad (6)$$

ΔE_{diss} , ΔH_{diss} and $T \cdot \Delta S_{\text{diss}}$ were calculated analogously to eq. (6).

The equilibrium constant was calculated from ΔG_{diss} using the respective ALD pressure as standard pressure:^{31,54,55}

$$\ln(K) = \frac{-\Delta_r G^\ominus(T)}{RT} = \frac{-\Delta G_{\text{diss}}(T)}{RT}. \quad (7)$$

With K, the dissociated dimer fraction (DDF) can be determined as shown in 6. in the SI by:

$$K = \frac{(2 \cdot \text{DDF})^2}{1 - \text{DDF}^2}. \quad (8)$$

leading to:

$$\text{DDF} = \sqrt{\frac{K}{K+4}}. \quad (9)$$

DDF is the ratio between the dimers that are dissociated, which is half of the amount of monomers n_{monomer} and the sum of the amount of dissociated and undissociated dimers n_{dimer} :

$$\text{DDF} = \frac{\frac{1}{2} n_{\text{monomer}}}{\frac{1}{2} n_{\text{monomer}} + n_{\text{dimer}}}. \quad (10)$$

Due to the linear temperature dependence of the Gibbs-energy and the logarithmic pressure dependence (see Fig. 4 and 5) it is straightforward to predict the ΔG_{diss} values under any condition as long as one variable is fixed. G under constant pressure is related to the temperature by:

$$\left(\frac{\partial G}{\partial T}\right)_p = -S. \quad (11)$$

The pressure dependence of G is:

$$\left(\frac{\partial G}{\partial p}\right)_T = V. \quad (12)$$

Because the volume V is related to the pressure it is not constant. Under ideal gas conditions, V is inversely related to p, which results in the logarithmic dependence between G and p.

$$V = \frac{nRT}{p}. \quad (13)$$

2.1.3 Energy decomposition analysis

Bonding analysis was performed with AMS 2023.101⁵⁶. The fragmentation was chosen in a way that each molecule in the dimer structure was one fragment in singlet ground-state. The EDA calculations were done with B3LYP⁴⁵⁻⁴⁷ and a DFT-D3^{38,39} dispersion correction. The slater type orbital (STO) type basis TZ2P^{57,58} was applied and the parameters of the numerical quality level

“good” were used. No relativistic effects were considered, and no frozen core approximation applied.

The EDA scheme applied in this study was developed by Morokuma⁵⁹ and by Ziegler and Rauk^{60,61}. The bond dissociation energy of two fragments A and B is the energy difference between the full molecule E_{AB} and the energies of the fragments in their relaxed geometry E_A^{rel} and E_B^{rel} :

$$E_{bond} = E_{AB} - E_A^{rel} - E_B^{rel} . \quad (14)$$

The EDA scheme separates the bonding energy into the preparation energy ΔE_{prep} and the interaction energy ΔE_{int} . The preparation energy is the energy needed for the deformation of the fragments from the relaxed state with energy E_A^{rel} and E_B^{rel} into the structure they have in the molecule with energies E_A and E_B :

$$E_{bond} = \Delta E_{prep} + \Delta E_{int} . \quad (15)$$

$$\Delta E_{prep} = E_A + E_B - E_A^{rel} - E_B^{rel} . \quad (16)$$

Consequently, the preparation energy ΔE_{prep} was calculated as energy difference between the fragments within the dimer geometry and the relaxed monomers. The interaction energy is further decomposed into a dispersion term $\Delta E_{int}(disp)$ and the electronic interaction energy $\Delta E_{int}(elec)$:

$$\Delta E_{int} = \Delta E_{int}(disp) + \Delta E_{int}(elec) . \quad (17)$$

The analysis finally decomposes the electronic interaction energy:

$$\Delta E_{int}(elec) = \Delta E_{Pauli} + \Delta E_{elstat} + \Delta E_{orb} . \quad (18)$$

The electrostatic term ΔE_{elstat} comprises the quasi-classical electrostatic interactions between the charge distributions and is usually attractive. The Pauli term ΔE_{Pauli} describes the repulsive effect due to normalization and antisymmetrisation of the resulting product wavefunction. The attractive orbital term ΔE_{orb} takes charge transfer and polarization effects into account.^{62–64} More detailed information on the presented EDA scheme can be found in the literature.^{65,66}

2.2 Computations for extended systems

Periodic slab calculations were performed with VASP 5.4.4^{67–71}, the PBE functional⁷² with D3(BJ)^{38,39} dispersion correction and a plane wave cutoff of 450 eV using standard PAWs⁷³. The Brillouin zone was sampled with a gamma-centered $\Gamma(2 \times 2 \times 1)$ Monkhorst-Pack^{74,75} mesh. The plane wave cutoff and k-grid were determined in a convergence test to an accuracy of 1 kJ·mol⁻¹ (see Fig. S1). The surface model was a crystalline, 3x3 α -quartz slab consisting of three O-Si-

layers where the bottom layer of silicon was H-terminated and kept frozen during the optimization. The top oxygen layer was saturated by hydrogen resulting in a hydroxylated silica surface. The cell parameters of the periodic cell are $a=16.550 \text{ \AA}$, $b=12.820 \text{ \AA}$, $c=22.000 \text{ \AA}$. The vacuum above the slab was set to 15 \AA . Minima were optimized with a conjugate gradient algorithm with a convergence criterium for the energy difference of the SCF cycle of 10^{-5} eV . The convergence criterium for the forces within the geometry optimization was set to $10^{-2} \text{ eV}\cdot\text{\AA}^{-1}$ for all optimizations. The slab was derived from an optimized SiO_2 bulk cell containing 3 silicon atoms and 6 oxygen atoms and cut along the (001) plane using VESTA 3.5.5⁷⁶. The bulk structure for optimization was obtained from the Crystallography Open Database.^{77,78} The parameters of the original bulk cell were $a=b=4.892 \text{ \AA}$, $c=5.389 \text{ \AA}$. The bulk was optimized with an energy cutoff of 500 eV and $\Gamma(5\times 5\times 5)$ k-point mesh. The parameters of the optimized bulk cell in the α -quartz phase were $a=b=4.934 \text{ \AA}$, $c=5.436 \text{ \AA}$.

Reaction paths were calculated with the nudged elastic band (NEB) method and transition states determined in a subsequent climbing image calculation (NEB-CI).^{79,80} Different to the optimization of minima, NEBs were optimized with the fast inertial relaxation engine (FIRE)⁸¹ and a tightened convergence criterium for the SCF cycle of 10^{-7} eV . To obtain the initial interpolation for the minimum energy path (MEP) as a starting point for the NEB, the image-dependent-pair-potential method⁸² (IDPP) was used. To check that the transition state had only one imaginary mode, a numeric frequency calculation was performed with finite differences of 0.015 \AA and an SCF convergence criterium of $10^{-5} \text{ eV}\cdot\text{\AA}^{-1}$.

3. Results and Discussion

In the first section we want to introduce the structures of the optimized dimers which are used in the second section to obtain accurate Gibbs free energies. Based on these, DDF under varying pressures and temperatures for each molecule are derived. In a third section, will discuss the thermochemistry at typical ALD conditions in detail. Here, results from our study will also be compared with previous data from the literature. To understand the observed trends of dimerization and allow predictions on the dimerization of Al-precursors we will then discuss a bonding analysis of the bridging dimer bond for all precursor classes in a fifth section. Finally, the adsorption behaviour of dimers compared to monomers and the possibility of dimer opening is tested on SiO₂.

3.1 Structures of dimerized precursors

Fig. 3 shows one representative example of the dimer structures from each substance class. The general structure of the dimerized precursors is the same for all molecules: All dimers show a four-membered ring that connects the two fragments containing the two aluminium atoms and two atoms from the ligands. The Al atom is either bonded to carbon (**1**) or to heteroatoms such as chlorine (**2**), nitrogen (**3**), and oxygen (**4**).

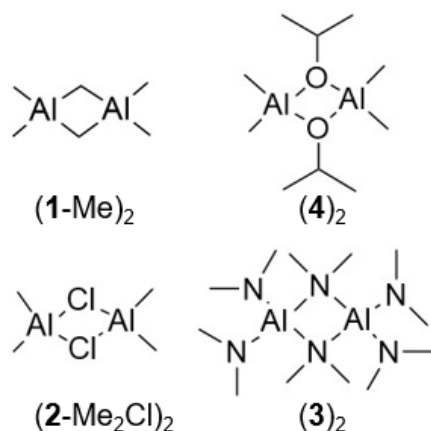


Figure 3. Dimer structures with one example of each substance class.

Structural parameters for the central 4-ring of the dimers are listed in Tab. 1. The distance between the Al atoms varies between 2.6 (**1**-iPr) and 3.3 Å (**2**-Me₂Cl). Here, the differences within each substance class are small and the Al-Al distance varies only by up to 0.1 Å. The distance between

Al and the second atom can be either the same, i.e. differences of less than 0.001 Å, such as in the case of (1-Me)₂ or different by 1.6 Å as with (1-iPr)₂ and (1-iBu)₂. If the distances are the same, it shows that the difference between the bond within one fragment and the bridging bond between the fragments has disappeared and the dimer has taken a symmetric form. As expected, this can be observed for the smaller dimers such as (1-Me)₂ and (2-Cl)₂ while the molecules with sterically more demanding groups such as 1-iPr cannot approach each other close enough for the dimer to take a symmetric form. Consequently, this comparison of the bond distances shows that not only the atoms directly involved in the bridging bonds but also the other atoms of the dimer have a significant influence on the dimer bond due to their steric demand.

Table 1. Structural parameters of the Al-X-Al-X (X=C, Cl, O, N) four-membered rings of the calculated precursor dimers.^[a]

Precursor	d(Al-Al)	d(Al-X) ^[b]	
1-Me	2.596	2.144	2.144
1-Et	2.578	2.189	2.142
1-Pr	2.576	2.199	2.134
1-iPr	2.567	2.317	2.153
1-iBu	2.627	2.254	2.092
2-Me ₂ Cl	3.281	2.332	2.331
2-MeCl ₂	3.237	2.304	2.304
2-Cl	3.185	2.279	2.279
3	2.823	1.854	1.853
4	2.805	1.984	1.968

[a] All bond distances in Å. Structures optimized at B3LYP-D3/def2-TZVPP.

[b] Some dimers exhibit asymmetric structures leading to two different bond lengths.

3.2 Pressure dependence of dimer dissociation

To analyse whether precursors are preferably monomeric or dimeric at certain conditions, the ΔG_{diss} values of the dimers were computed. If ΔG_{diss} is positive, the dimers are thermodynamically favoured while a negative value shows a thermodynamic driving force for dissociation. Furthermore, equilibrium constants and DDFs were derived from ΔG_{diss} . The ΔG_{diss} values of **1-4** as function of the pressure are shown in Fig. 4. Here, a range of typical ALD pressures (“ALD window”) from 10^{-4} to 10^{-2} bar^{14,15,29,30} is highlighted.

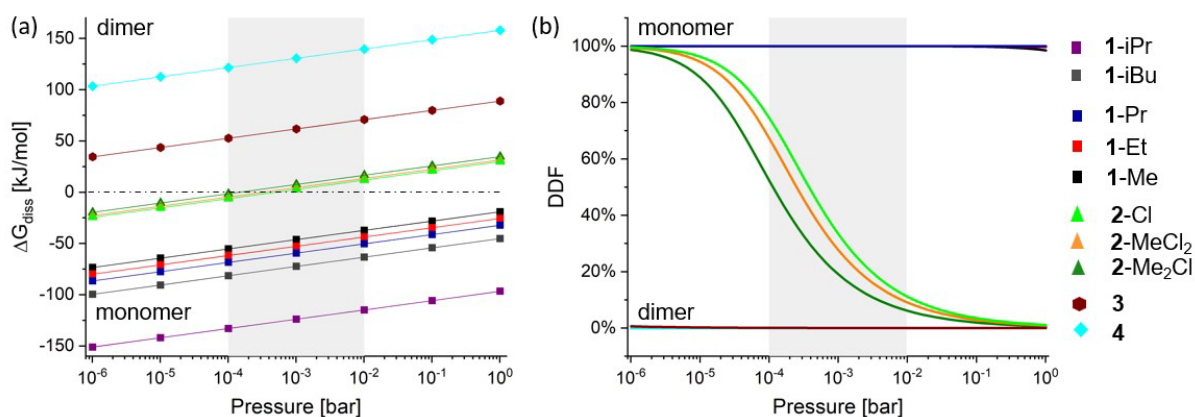


Figure 4. (a) Gibbs free energy of dissociation (ΔG_{diss}) as function of pressure at $T = 200^\circ\text{C}$ for **1-4**. (b) Dissociated dimer fraction (DDF) as function of pressure at 200°C for the tested set of Al-precursors. Common ALD pressures from 10^{-4} to 10^{-2} bar are highlighted in grey.

For the whole range of pressures from 10^{-6} to 1 bar, ΔG_{diss} is negative for all five aluminum-alkyls of group **1**. Dimers of **3** and **4** have positive ΔG_{diss} at the given pressures and only the chlorinated precursors of group **2** change the sign of the ΔG_{diss} values between 10^{-3} and 10^{-4} bar. Consequently, **3** and **4** are preferably dimeric, the alkyl precursors monomeric and the chlorinated compounds are preferably monomeric at pressures below 10^{-4} bar or preferably dimeric at higher pressures above 10^{-3} bar. Another observation is that the number of Cl atoms of the chlorinated compounds has little influence on the thermodynamic driving force of dimerization. ΔG_{diss} values differ only by up to $\Delta\Delta G_{\text{diss}} = 5 \text{ kJ}\cdot\text{mol}^{-1}$ for the **2-Me₂Cl**, **2-MeCl₂** and **2-Cl** precursor. The more Cl atoms the compound contains, the lower ΔG_{diss} becomes. The length of alkyl chains has a greater impact on ΔG_{diss} than the number of Cl atoms. Here, the difference between **1-Me** and **1-Pr** is $\Delta\Delta G_{\text{diss}} = 13 \text{ kJ}\cdot\text{mol}^{-1}$. The longer the alkyl chains, the lower ΔG_{diss} becomes and the more is the monomeric form preferred. Still, the observation that the compound class has a higher influence than the substitution pattern remains valid as the maximum difference of precursors of group **2** to precursors of group **1** is $\Delta\Delta G_{\text{diss}} = 49 \text{ kJ}\cdot\text{mol}^{-1}$. An even higher difference is observed for precursor classes **2** to **3** with $\Delta\Delta G_{\text{diss}} = 54 \text{ kJ}\cdot\text{mol}^{-1}$. The observation that the differences between the different compound classes are relatively high compared to the differences within each compound class is not unexpected as the atoms in the bridging dimer bond are different for each class of precursors. The only exception here are the branched aluminum alkyls, especially **1-iPr**. With $\Delta\Delta G_{\text{diss}} = 64 \text{ kJ}\cdot\text{mol}^{-1}$ between **1-iPr** and its isomer **1-Pr** the difference is exceptionally large. Branching thus makes dimerization much less favorable. This effect is explained by the steric repulsion of the

branched ligands that weakens the dimer bond. A more detailed analysis of the effect of different alkyl chains is shown by the EDA analysis in section 3.6. While the atoms involved in the dimer bond are in general the most important influence on the dimer bond, the influence of the other atoms can be significant as already discussed with the structural parameters in 3.1.

Given the ΔG_{diss} values, the DDF was calculated as described in section 2.1. Figure 4 (b) shows the DDF at different pressures for each precursor at $T = 200^\circ\text{C}$. In the relevant range of pressures from 10^{-4} to 10^{-2} bar, no dissociation of dimers of precursors **3** and **4** is visible. The aluminum alkyls of group **1** are completely dissociated, and dimers begin to form only at pressures close to atmospheric conditions, which is far beyond common ALD conditions. The chlorinated compounds of group **2** make a transition from almost complete dissociation at 10^{-6} bar to almost undissociated dimers at atmospheric conditions. At 10^{-3} bar the DDF of the chlorinated dimers ranges from 19% (**2-Me₂Cl**) to 33% (**2-Cl**). It is worth to mention that in case of **2-Cl** and **2-MeCl₂** the transition from a majority to a minority of dissociated dimers happens in the ALD window between 10^{-4} and 10^{-2} bar.

The general relation derived from the graph between ΔG_{diss} values and the pressure p in bar can be described by the following formula:

$$\Delta G_{\text{diss}} \left[\frac{\text{kJ}}{\text{mol}} \right] = RT \cdot \ln(p) + b \quad (19)$$

R is the universal gas constant and T the temperature of 473 K (200°C). The parameter b is shown in Tab. S8 in the supporting information for each precursor. This enables a derivation of ΔG_{diss} for other pressure values than shown in Fig. 4 for future ALD studies.

3.3 Temperature dependence of dimer dissociation

Apart from the pressure dependency of the dissociation also the temperature dependency was investigated. Fig. 5 shows ΔG_{diss} and the DDF for all precursor dimers. Again, a typical range of ALD temperatures from 100 to 300°C ³ is highlighted.

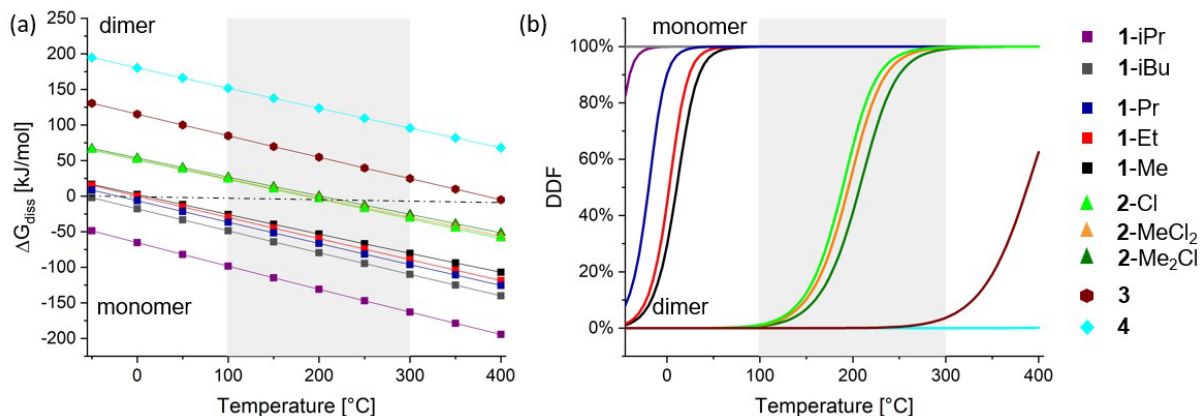


Figure 5. (a) Gibbs free energy of dissociation (ΔG_{diss}) in dependence of the temperature for the discussed set of precursors at a pressure of $1.73 \cdot 10^{-4}$ bar (130 mTorr). (b) Dissociated dimer fraction (DDF) versus temperature at $1.73 \cdot 10^{-4}$ bar (130 mTorr) for the tested set of Al-precursors. A common temperature range for ALD is highlighted in grey.

3 and **4** have positive ΔG_{diss} values from $T = -50^{\circ}\text{C}$ to nearly 400°C and in case of the chlorinated precursors of group **2**, the sign of ΔG_{diss} changes at 200°C . For the precursors with linear alkyl chains of group **1** the ΔG_{diss} values are negative at temperatures above 0°C while the sign changes to positive ΔG_{diss} values at lower temperatures. The precursors with branched alkyl chains **1-iPr** and **1-iBu** have a negative ΔG_{diss} over the whole range of temperatures from -50 to 400°C . It needs to be considered that the pressure in our study is far below standard pressures of 1.013 bar (1 atm). At a higher pressure, dimerization becomes more favorable as shown in the previous section 3.2, enabling dimerization at even higher temperatures. Consequently, this explains that dimers of **1-Me** have been identified in experiment at higher pressures and temperatures below 100°C .^{22,83} As observed before for the pressure-dependence, the influence of the substance class is stronger than that of the number of Cl atoms or the alkyl chain length. While the alkyl chain length makes a difference of up to $\Delta\Delta G_{\text{diss}} = 18 \text{ kJ}\cdot\text{mol}^{-1}$ and the number of chlorine atoms up to $\Delta\Delta G_{\text{diss}} = 7 \text{ kJ}\cdot\text{mol}^{-1}$ at 400°C , the maximum difference between substance classes (**2-Cl** and **1-Me**) is $\Delta\Delta G_{\text{diss}} = 48 \text{ kJ}\cdot\text{mol}^{-1}$ at this temperature. As the transition between the monomeric and dimeric form of group **2** takes place at typical ALD conditions this property is interesting for applications because it opens the possibility to control the state of the precursor (monomer or dimer) by adjusting the process conditions like the temperature and pressure applied in the ALD process. This would allow to influence the reactivity of the precursors in a targeted way. In the same way as discussed before

a higher number of Cl atoms or a higher alkyl chain length leads to slightly lower ΔG_{diss} values which shifts the equilibrium towards the monomeric form.

From the ΔG_{diss} values the DDFs were calculated as described in section 2.1.2. Fig. 5 shows the dissociated dimer fraction from -50 to 400°C that was calculated according to equation (9) for each precursor. The result shows that the alkyl-based precursors of group **1** undergo the transition from dimer to monomer before the typical ALD window whereas the chlorinated precursors of group **2** show this transition within the ALD window. **4** remains stable as a dimer over the whole temperature range whereas **3** starts to dissociate at above 250 °C.

The general relation derived from the graph between the calculated ΔG_{diss} values and temperature T in °C can be described by the following formula:

$$\Delta G_{\text{diss}} \left[\frac{\text{kJ}}{\text{mol}} \right] = -a \cdot T + b \quad (20)$$

The parameters a and b are shown in Tab. S9 in the supporting information for each precursor. This enables a derivation of ΔG_{diss} for other temperature values than shown in Fig. 5 for future ALD studies.

3.4 Thermochemistry for typical ALD conditions

After presenting the temperature and pressure dependence of ΔG_{diss} and DDFs for a range of temperatures and pressures, a detailed analysis of all relevant parameters (ΔE_{diss} , ΔH_{diss} , ΔG_{diss} , ΔS_{diss} , DDF, K) for one set of temperature (200°C) and pressure ($1.73 \cdot 10^{-4}$ bar, 130 mTorr) is presented in Tab. 2.

Table 2. Compiled thermochemical data of the dissociation reaction of the dimers at ALD conditions of $T=200^{\circ}\text{C}$ and $p=1.73\cdot 10^{-4}$ bar (130 mTorr).^[a]

	1-iBu	1-iPr	1-Me	1-Et	1-Pr	2-Me₂Cl	2-MeCl₂	2-Cl	3	4
ΔE_{diss}	80.0	46.3	91.1	94.9	88.0	132.4	129.0	127.9	205.8	266.6
ΔH_{diss}	65.1	28.1	80.5	81.8	73.8	124.2	121.2	120.3	194.9	257.1
$-T\cdot\Delta S_{\text{diss}}$	-144.5	-159.0	-133.8	-141.6	-140.2	-123.7	-123.8	-124.5	-140.1	-133.5
ΔG_{diss}	-79.4	-130.9	-53.2	-59.7	-66.4	0.5	-2.6	-4.2	54.8	123.6
$K^{[b]}$	5.9E+08	2.9E+14	7.5E+05	3.9E+06	2.2E+07	8.8E-01	1.9E+00	2.9E+00	8.9E-07	2.2E-14
$\ln K^{[c]}$	20.19	33.28	13.53	15.18	16.88	-0.13	0.66	1.07	-13.93	-31.43
DDF	100.00%	100.00%	100.00%	100.00%	100.00%	42.48%	57.12%	64.89%	0.05%	0.00%

[a] All ΔE , ΔH , ΔG and $-T\cdot\Delta S$ values in $\text{kJ}\cdot\text{mol}^{-1}$, as defined in section 2.1.3

[b] Equilibrium constant K of the dissociation reaction illustrated in Fig. 1

[c] The logarithm of K is directly proportional to ΔG_{diss} according to eq. (7)

As previously discussed, all dimers of the precursors of group **1** are dissociated at the selected conditions. In the same way, all dimers of **4** are intact. **3** also remains largely undissociated with only 0.05% DDF according to the calculation. Whether the monomeric form would already play a role with such a degree of dissociation in experiment or be negligible cannot be predicted easily. At least the values show that the dimers of **4** are slightly more stable than the dimers of **3**.

Furthermore, the table gives insight into the different terms of ΔG_{diss} and one may ask which are decisive to explain the trends found in ΔG_{diss} . Considering ΔH_{diss} , it is evident that almost the same trend as that of ΔG_{diss} is observed. The only exception is the ordering of **1-Me** and **1-Et**. Here, ΔH_{diss} of **1-Me** is slightly higher by $\Delta\Delta H_{\text{diss}} = 1.3 \text{ kJ}\cdot\text{mol}^{-1}$ compared to **1-Et**. The corresponding ΔG_{diss} of **1-Me** is lower by $\Delta\Delta G_{\text{diss}} = 6.5 \text{ kJ}\cdot\text{mol}^{-1}$ compared to **1-Et**. The entropy term $-T\cdot\Delta S_{\text{diss}}$ correlates less with ΔG_{diss} . For example, the same order for $-T\cdot\Delta S_{\text{diss}}$ and ΔG_{diss} is observed within group **2**, while $-T\cdot\Delta S_{\text{diss}}$ for **3** and **4** is lower than for any precursor of group **2** and thereby in contrast to the trend of ΔG_{diss} . Consequently, the enthalpy ΔH_{diss} is a better measure for the dimer stability than the entropy term $-T\cdot\Delta S_{\text{diss}}$ and allows more predictions on the relative stability of dimers. Still, both terms are essential to predict whether a compound is monomeric or dimeric under certain conditions.

From a computational point of view, the data in Tab. 2 greatly show the need for accurate computational methods. While the dimers of **2-Me₂Cl** and **2-Cl** differ only by $\Delta\Delta G_{\text{diss}} = 3.7$

$\text{kJ}\cdot\text{mol}^{-1}$ a qualitative difference in the DDF value is present as it is changing from 42% in case of **2**-Me₂Cl to 65 % for **2**-Cl. Thus, a difference of $\Delta\Delta G_{\text{diss}} < 4 \text{ kJ}\cdot\text{mol}^{-1}$ leads to a difference of more than 20% in the DDF. This sensitivity of the DDF on the ΔG_{diss} value is a consequence of the exponential relationship between ΔG_{diss} and K (see eq. (7)), which is used for the calculation of the DDFs (eq. (9)). Tab. S10 in the supporting information further supports this finding as it shows a comparison of the values presented above to values derived with DFT instead of CCSD(T) energies.

3.5 Comparison with previous data on precursor dimerization

To evaluate the impact of an improved theoretical approach and reasonable ALD pressures on the thermochemistry predictions, a comparison with previous calculations is made. Oh et al.¹⁴ determined the thermochemistry for **1**-Me, **1**-Et, **2**-Me₂Cl, **2**-MeCl₂ and **2**-Cl using DFT approaches. A comparison of the ΔG_{diss} and the DDF values to our results is shown in Tab. 3. It needs to be noted that the formula for the calculation of the DDF from the equilibrium constant applied by Oh et al.¹⁴ differs from our calculation. The impact of this difference is discussed in the SI (see Fig. S2 and S3).

Table 3. Comparison of calculated ΔG_{diss} and DDFs of the chlorinated precursors of group **2** as well as **1**-Me and **1**-Et to literature data.^[a]

Value	Reference	Method	p	2 -Cl	2 -MeCl ₂	2 -Me ₂ Cl	1 -Me	1 -Et
ΔG_{diss}	Oh et al. ^[b]	DFT	1.013 bar	25.6	18.3	22.9	-31.0	-29.7
	This study ^[c]	DFT	1.013 bar	31.5	30.7	31.3	-27.9	-33.9
	This study ^[d]	CCSD(T)	1.013 bar	29.9	31.5	34.6	-19.1	-25.6
	This study ^[d]	CCSD(T)	$1.73\cdot 10^{-4}$ bar	-4.2	-2.6	0.5	-53.2	-59.7
DDF	Oh et al. ^[b]	DFT	1.013 bar	1.0%	3.5%	1.2%	99.8%	99.8%
	This study ^[c]	DFT	1.013 bar	0.9%	1.0%	0.9%	99.8%	100.0%
	This study ^[d]	CCSD(T)	1.013 bar	1.1%	0.9%	0.6%	98.5%	99.7%
	This study ^[d]	CCSD(T)	$1.73\cdot 10^{-4}$ bar	64.9%	57.1%	42.5%	100.0%	100.0%

[a] All ΔG values in $\text{kJ}\cdot\text{mol}^{-1}$.

[c] Values derived at 200°C 1.013 bar, $75.98\cdot 10^4$ mTorr using B3LYP-D3/6-311G**.

[b] Values calculated with B3LYP-D3/def2-TZVPP.

[d] Values calculated based on the CCSD(T)-based protocol outlined above.

Our most accurate values for the ΔG_{diss} at $1.73 \cdot 10^{-4}$ bar (130 mTorr) differ significantly from the values from literature. For **2-Cl**, for example, a ΔG_{diss} value of $-4.2 \text{ kJ}\cdot\text{mol}^{-1}$ was determined in our study compared to a value of $25.6 \text{ kJ}\cdot\text{mol}^{-1}$ by Oh et al.¹⁴ what makes a difference of $29.8 \text{ kJ}\cdot\text{mol}^{-1}$. In addition, the DDF prediction differs significantly for group **2**: While the chlorinated precursors are only partially dissociated with 1.0 to 3.5% according to Oh et al.¹⁴, it can reach values of up to 64.9% (**2-Cl**) in our study. For **1-Me** and **1-Et** the differences in ΔG_{diss} are with $\Delta\Delta G_{\text{diss}} = 22.2 \text{ kJ}\cdot\text{mol}^{-1}$ and $\Delta\Delta G_{\text{diss}} = 30.0 \text{ kJ}\cdot\text{mol}^{-1}$ still significant. However, since a DDF of 100% observed in our study cannot be exceeded, similar values of 99.8% are observed by Oh et al.¹⁴. Overall, all ΔG_{diss} values calculated at $1.73 \cdot 10^{-4}$ bar (130 mTorr) are lower compared to the values from Oh et al.¹⁴ leading to higher DDFs.

The pressure values used in the calculations are the main reason to explain the observed differences. If 1.013 bar ($75.98 \cdot 10^4$ mTorr) is used instead of typical ALD pressures, ΔG_{diss} becomes closer to the values from Oh et al.¹⁴. This is especially the case for the chlorinated precursors. At standard pressure, a ΔG_{diss} value of $29.9 \text{ kJ}\cdot\text{mol}^{-1}$ has been obtained for **2-Cl** in our study compared to $25.6 \text{ kJ}\cdot\text{mol}^{-1}$ by Oh et al.¹⁴. This makes a difference of only $\Delta\Delta G_{\text{diss}} = 4.3 \text{ kJ}\cdot\text{mol}^{-1}$ compared to a difference of $\Delta\Delta G_{\text{diss}} = 29.8 \text{ kJ}\cdot\text{mol}^{-1}$ when lower pressures of $1.73 \cdot 10^{-4}$ bar (130 mTorr) are applied.

The use of B3LYP-D3 only instead of the combined approach with CCSD(T) did not always lead to results that were closer to that in the literature. Only for **1-Me** the value of $-27.9 \text{ kJ}\cdot\text{mol}^{-1}$ is considerably closer to the value of $31.0 \text{ kJ}\cdot\text{mol}^{-1}$ calculated by Oh et al.¹⁴ compared to $-19.1 \text{ kJ}\cdot\text{mol}^{-1}$ with the combined approach. We attribute the remaining differences between our and the calculations of Oh et al. to different conformers and the different basis sets. Tab. S7 shows an overview of common errors from DFT calculations, and the errors estimated from the method tests that are described in section 2. in the supporting information. The comparison shows how the methodology of ab initio calculations on dimerization can affect the predicted dissociation. The application of typical ALD pressures and a refined methodology gives considerably different results. A further comparison between the method applied in the study presented here and a “standard” - DFT approach is shown in Tab. S10 in the SI.

While the comparison above includes only the precursors of class **1** and **2**, also theoretical data on the dissociation of (**4**)₂ are available. Kim et al.⁸⁴ calculated the dimerization energy (ΔE_{dim}) of **1-Me** and **4** with machine-learning potentials (MLP) and compared the result with DFT calculations

using the PBE functional. In the same way the Gibbs free energy for the dimerization (ΔG_{dim}) was calculated and compared for a temperature range of -73°C to 473°C (200 to 600 K) at $1.33 \cdot 10^{-3}$ bar (1000 mTorr).

An electronic energy of $-104 \text{ kJ}\cdot\text{mol}^{-1}$ (-1.08 eV) for the dimerization of **1**-Me and of $-250 \text{ kJ}\cdot\text{mol}^{-1}$ (-2.59 eV) for the dimerization of **4** was calculated with the MLP. The dimerization energies from PBE were slightly different with $-94 \text{ kJ}\cdot\text{mol}^{-1}$ (-0.97 eV) in case of **1**-Me and $-239 \text{ kJ}\cdot\text{mol}^{-1}$ (-2.48 eV) in case of **4**. In our study the dimerization energy of **1**-Me is $-91 \text{ kJ}\cdot\text{mol}^{-1}$ and $-267 \text{ kJ}\cdot\text{mol}^{-1}$ for **4** what makes the **1**-Me dimer slightly weaker ($-10 \text{ kJ}\cdot\text{mol}^{-1}$ difference) associated compared to the MLP result and the **4** dimer slightly stronger ($+17 \text{ kJ}\cdot\text{mol}^{-1}$ difference) associated. The general chemical trend is the same, however. Tab. 4 shows the comparison of the electronic dimerization energies of our study with those calculated by Kim et al.⁸⁴ The differences to our values can be explained by the use of a different calculation method; the MLP had been trained on the basis of PBE-results. With B3LYP-D3 and CCSD(T) the results from the study presented in our paper can be assumed to be more accurate.

Table 4. Dimerisation energies (ΔE_{dim}) of **1**-Me and **4**.^[a]

Reference	Method	1 -Me	4
This study ^[b]	CCSD(T)	-91	-267
Kim et al. ^[c]	MLP	-104	-250
Kim et al. ^[d]	DFT	-94	-239

[a] All values in $\text{kJ}\cdot\text{mol}^{-1}$.

[b] Values calculated based on the CCSD(T)-based protocol outlined above.

[c] Values calculated with a universal MLP (PreFerredPotential) trained on data from PBE-D3 and the PAW approach.

[d] Values calculated with PBE-D3 and the PAW approach.

The ΔG values for the dimerization (ΔG_{dim}) from MLP calculated by Kim et al.⁸⁴ predict **4** to be dimeric at the whole temperature range from -73°C to 473°C (200 to 600 K) at $1.33 \cdot 10^{-3}$ bar (1000 Torr). Only the DFT results predict a transition from the dimeric to the monomeric form at about 473°C where ΔG gets slightly positive. **1**-Me has a positive ΔG_{dim} above 27°C (300 K) what means that the monomer is preferred and a negative ΔG_{dim} below that temperature according to MLP and DFT results. Our study predicts (**4**)₂ to be dimeric over the range of -50 to 400°C (see Fig. 5) as well and **1**-Me to make a transition from dimer to monomer between -50 and $+100^{\circ}\text{C}$ and being completely dissociated above 100°C . ΔG_{dim} changes sign between 5 and 10°C according to our results what is at lower temperature than in the study of Kim et al.⁸⁴ The earlier dissociation

of **1-Me** is not in contradiction with their results because the pressure at which the thermochemistry was calculated was with $1.73 \cdot 10^{-4}$ bar lower in our study and therefore the equilibrium is shifted towards the monomer. With this, both studies give the same qualitative predictions for the given range of temperatures.

Furthermore, to check whether the calculations make realistic predictions about dimerization, a comparison with experimental results on dimer dissociation is made. According to Almenningen et al.²² **1-Me** is 97% dimeric at 0.04 bar (30000 mTorr) and 60°C while it is 96% monomeric at 215°C. The DDF in our approach according to equation (9) is 41% at 60°C and 0.04 bar and 100% at 215°C and 0.04 bar (30000 mTorr). The qualitative transition from a majority of dimer to almost complete dissociation agrees with the experimental result whereas the degree of dissociation that is predicted is different. This could be either due to limitations of the theoretical method, like approximations made in the calculation of the thermochemistry, or due to inaccuracies of the experiment. Further experimental data would be needed to evaluate the reliability of the theoretical method for the quantitative prediction of the DDF.

A further comparison with experiment is done on the structure of the dimers on the example of (**1-Me**)₂ in the SI (See Fig. S4 and Tab. S11).

3.6 EDA on dimer bond

To get an understanding of the chemical origin of the differences in dimerization degree for the investigated set of precursors, EDA calculations were performed on the dimer bond. The energy decomposition analysis should help to identify reasons and trends for the different bond strengths to make predictions on the dimerization of new precursor compounds or compound classes. Fig. 6 shows the most important result of the EDA calculations on the dimer bond for each class of precursor. The complete dataset is shown in Tab. S12 and Fig. S5 in the supporting information.

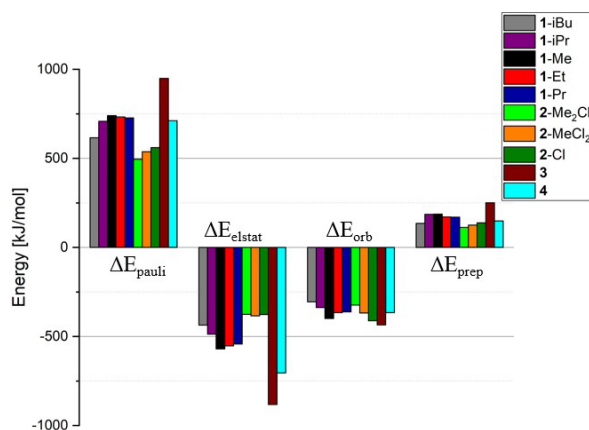


Figure 6. EDA on the dimer bond of the Al-precursors. All energy terms are shown in $\text{kJ}\cdot\text{mol}^{-1}$.

The preparation energy (ΔE_{prep}) in general increases by the order $2 < 1 \approx 4 < 3$. With an increasing ΔE_{prep} term, more energy is needed to deform the monomer fragments into the dimer geometry. The preparation energy of **1-Me** is highest compared to the other precursors of class **1**. That means that larger bulkiness of the alkyl groups does not necessarily lead to a higher ΔE_{prep} as one might have expected.

The Pauli repulsion (ΔE_{pauli}) of the chlorinated precursors of group **2** is smaller than that of the other compounds. It is highest in case of **3**. It is worth to be mentioned that ΔE_{pauli} in substance class **1** is strongest for **1-Me** again. **1-iBu** in contrast has the lowest ΔE_{pauli} of precursor class **1**. The bulkiness of the alkyl ligands leads not to a higher Pauli repulsion. This can be explained by increasing bond lengths (see Tab. 1) of the dimers with branched alkyl chains. The bulkiness of the ligands increases the length of the dimer bond and thereby minimizes ΔE_{pauli} . Similarly to the Pauli repulsion, the electrostatic interaction (ΔE_{elstat}) is strongest in case of **3**. This compensates the high ΔE_{pauli} and allows for the formation of a stable dimer bond. Both **4** and **3** show with -705 and $-882 \text{ kJ}\cdot\text{mol}^{-1}$ of ΔE_{elstat} a stronger electrostatic attraction than all other precursors that reach only values of up to $-570 \text{ kJ}\cdot\text{mol}^{-1}$ (**1-Me**). The orbital terms, in contrast, are rather similar for all compound classes with -305 (**1-iBu**) to $-435 \text{ kJ}\cdot\text{mol}^{-1}$ (**3**).

A diagram with all terms of the EDA is shown in Fig. S5. As a sum of all terms, the absolute value of the bonding energy (ΔE_{bond}) increases as expected by the order $1 < 2 < 3 < 4$. The dispersion term (ΔE_{disp}) is relatively small compared to the other terms and therefore not decisive and is not

discussed here. Therefore, the terms shown in Fig. 6 are mainly responsible for the observed trend in ΔE_{bond} and with that the dimer stability of the different substance classes.

From EDA, the following conclusions about the stability of dimer bonds are drawn: First, alkyl groups are unfavorable as bridging ligands because of their high ΔE_{pauli} and ΔE_{prep} . This affects not only relatively bulky ligands as iso-butyl but also small ligands like methyl. A stable dimer bond can be achieved with heteroatoms containing a free electron pair as O and N that stabilizes the bond to Al due to ΔE_{elstat} . Chlorine, as bigger atom of the third period, behaves differently, however. This is explained by the larger size of the atom leading to a more diffuse electron density. Another difference to the other groups is that no deformation of chlorine as a single atom is possible, different to ligands that consist of more atoms. This explains the low ΔE_{prep} value of the chlorinated precursors. With chlorine, all terms except ΔE_{orb} , including the attractive ΔE_{elstat} as well as the terms that weaken the bond are comparably small. This leads to ΔE_{bond} between that of the precursor class **1** and the precursors of **3** and **4**. As a conclusion, the substance class and thereby the atoms involved in the bridging dimer bond determines the nature and strength of the dimer bond while the substitution within a class is less relevant. Consequently, to predict whether a precursor is dimeric, the bridging atoms are decisive rather than the absolute size or bulkiness of the ligands.

3.7 Dimer versus monomer adsorption

Finally, after determining which precursor is prevalent in which form the question is addressed which impact the dimerization has on ALD processes. The formation of dimers might lead to a lower chemical reactivity of precursors. This can be especially relevant for AS-ALD processes where undesired material deposition needs to be avoided. Furthermore, the higher molecular volume of dimers can make reactive surface sites less accessible to the precursor molecule. In AS-ALD, even physisorption of precursors might lead to undesired nucleation of material on the non-growth surface.⁸⁵

To get an impression about the adsorption of dimers compared to the corresponding monomers, calculations including a hydroxylated silica surface model were performed. The structures of **1**-Me, **2**-Cl, and **4** as representative examples for the different substances and their dimers above the surface were calculated.

Here, monomers and dimers were considered independent of their likelihood to be present in experiment to compare their reactivities and explore the impact of the dimerization on surface reactivity. Understanding this dimerization-reactivity relation in combination with the knowledge of the preferred form at common conditions can help to understand why certain precursors are rather reactive or unreactive in AS-ALD applications. Furthermore, as in the case of the chlorinated precursors the knowledge of the conditions for dimerization could even allow to influence their reactivities by choosing the desired precursor form by tuning the process conditions. While this study gives a limited impression on the reactivity of dimers further investigations will be necessary to confirm what chemical intuition and adsorption structures on the surface indicate. Fig. 7 shows the adsorbing dimers and monomers including bond length and adsorption energies.

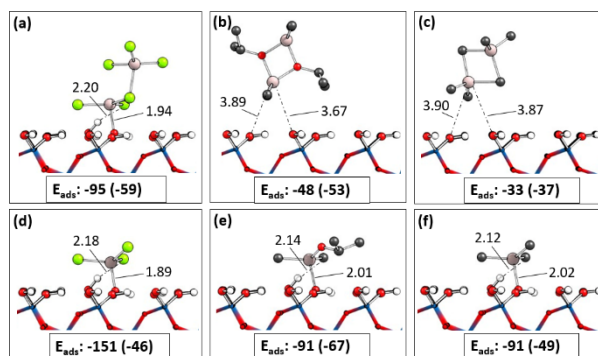


Figure 7. Adsorption of dimers a) $(2\text{-Cl})_2$, b) $(4)_2$, c) $(1\text{-Me})_2$ and monomers d) 2-Cl , e) 4 , f) 1-Me on SiO_2 . Bond lengths are shown in Å and adsorption energies in $\text{kJ}\cdot\text{mol}^{-1}$. The dispersion contribution to the adsorption energy is shown in brackets. Color code: (soft) pink – Al, green – Cl, black – C, red – O, white - H. All hydrogens attached to carbon are omitted for clarity.

The absolute value of adsorption energy (E_{ads}) is higher for the monomers than the dimers in all three cases with a difference exceeding $+40 \text{ kJ}\cdot\text{mol}^{-1}$ for all molecules. In terms of bond strength, 2-Cl (Fig. 10d) adsorbs strongest with E_{ads} of $-151 \text{ kJ}\cdot\text{mol}^{-1}$ whereas its dimer is adsorbed with only $-95 \text{ kJ}\cdot\text{mol}^{-1}$ (Fig. 10a). In comparison, 4 and 1-Me form a chemical bond as monomers with slightly higher adsorption energies of $-91 \text{ kJ}\cdot\text{mol}^{-1}$ each while their dimers are only weakly bound by dispersion interactions leading to E_{ads} of $-48 \text{ kJ}\cdot\text{mol}^{-1}$ for $(4)_2$ and $-33 \text{ kJ}\cdot\text{mol}^{-1}$ with $(1\text{-Me})_2$, respectively.

The trend in adsorption energies is also reflected in the adsorption structures. The bonds to the surface are generally longer in case of the dimers compared to the monomers. The dimer of 2-Cl

has a 0.05 Å longer bond to the surface than the monomer. The difference is considerably higher with **1**-Me and **4**. The dimers of **1**-Me and **4** are more than 3 Å above the surface, whereas the monomers have a bond length of around 2.0 Å to the surface. A decomposition of (**1**-Me)₂ and (**4**)₂ does not take place. In case of (**2**-Cl)₂ one bond of the dimer breaks due to the adsorption to the surface.

The comparison of bond lengths and adsorption energies (E_{ads}) shows that (**2**-Cl)₂ binds different than the other dimers. While **1**-Me and **4** are only weakly adsorbed by dispersion, (**2**-Cl)₂ can form an actual covalent bond to the surface. This shows that the chlorinated precursors might adsorb even as dimers as good to the surface as other precursors and their dimerization might therefore not prevent undesired reactions with surfaces. This is because precursor adsorption to the non-growth area plays a key role in the loss of selectivity in AS-ALD and is therefore to be prevented.¹⁷ That **2**-Cl adsorbs to the surface so strongly might be explained by the high Lewis-acidity of the Al-atom and the possibility to break the dimer bond with a reasonable amount of energy. In contrast to that, the alkyl- substituted precursors of group **1** are less Lewis acidic because they have no electron withdrawing groups whereas **3** and **4** might have such groups but form more stable dimers than the chlorinated precursors of class **2**. In case of **4** and **1**-Me, the dimers show little interaction with the surface and due to the high stability, no high chemical reactivity is expected for (**4**)₂. The monomers, in contrast, can bind to the surface what shows the chemical difference and therefore the relevance of the dimerization question for the precursor chemistry. The reactivity comparison between monomers and dimers is an interesting avenue for future computational explorations of precursor-surface interactions.

In AS-ALD not only the interaction between Al-precursors with the surface but also with SMIs can be relevant. Here, trimethoxypropylsilane (TMPS) was chosen as inhibitor for the SiO₂-surface, which has been investigated experimentally and theoretically in previous studies.¹⁶ Fig. 8 shows the adsorption of the three molecules as dimers and monomers to a methoxy-group of the TMPS inhibitor bound to the SiO₂ surface.

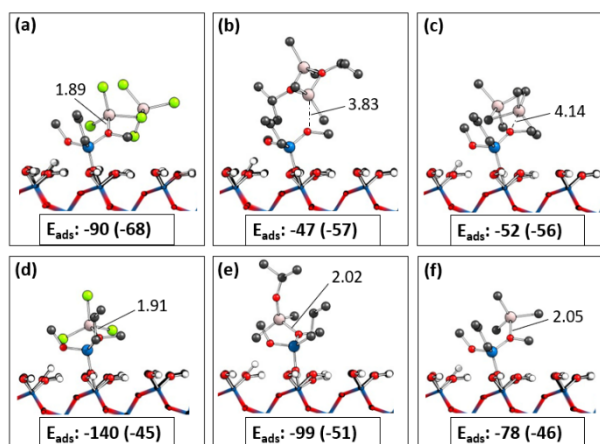


Figure 8. Adsorption of dimers a) $(2\text{-Cl})_2$, b) $(4)_2$, c) $(1\text{-Me})_2$ and monomers d) 2-Cl , e) 4 , f) 1-Me on the methoxy group of the small molecule inhibitor TMPS. Bond lengths are shown in Å and adsorption energies in $\text{kJ}\cdot\text{mol}^{-1}$. The dispersion contribution to the adsorption energy is shown in brackets. Color code: (Soft) pink – Al, green – Cl, black – C, red – O, white - H. All hydrogens attached to carbon are omitted for clarity.

Again, the monomers adsorb with a higher absolute value of E_{ads} than the dimers. 2-Cl adsorbs strongest of all three precursors with E_{ads} of $-140 \text{ kJ}\cdot\text{mol}^{-1}$ whereas its dimer $(2\text{-Cl})_2$ is only bound by $-90 \text{ kJ}\cdot\text{mol}^{-1}$. The monomers of 1-Me and 4 are weaker bound to the surface than 2-Cl with $-99 \text{ kJ}\cdot\text{mol}^{-1}$ (1-Me) and $-78 \text{ kJ}\cdot\text{mol}^{-1}$ (4). The dimers $(1\text{-Me})_2$ and $(4)_2$ are again only slightly adsorbed by dispersion interactions with adsorption energies of $-47 \text{ kJ}\cdot\text{mol}^{-1}$ in case of $(1\text{-Me})_2$ and $-52 \text{ kJ}\cdot\text{mol}^{-1}$ for $(4)_2$. The bond lengths are longest with the dimers $(1\text{-Me})_2$ and $(4)_2$ with 3.83 Å in case of $(1\text{-Me})_2$ and 4.14 Å in case of $(4)_2$. Their monomers are again adsorbed with a bond length of around 2 Å (1-Me : 2.05 Å , 4 : 2.02 Å). Different to these two precursors, 2-Cl binds with approximately the same length as monomer like as dimer. The distance of the Al atom to the methoxy group measures 1.91 Å in case of the monomer of 2-Cl and is even a bit shorter with 1.89 Å for the dimer.

The comparison of adsorption structures and energies shows that the monomers bind chemically to the methoxy group while only in case of 2-Cl the dimer binds chemically, too. Like with the pristine SiO_2 surface the dimers of 1-Me and 4 are only physisorbed. In general, a similar result compared to the pure SiO_2 surface was observed for the adsorption to TMPS molecules.

The adsorption tests on SiO_2 and to TMPS as inhibitor on SiO_2 both confirm the expectation that monomers behave chemically different to dimers and that dimers have less chemical interaction with inhibitors and the surface. However, it depends on the type of precursor to which degree dimers interact. While $(2\text{-Cl})_2$ can open and form chemical bonds, the dimers of 1-Me and 4 have

shown to be rather inert in this small test series. The differences in adsorption behavior indicate that dimerization can play a key role for the precursor selectivity in AS-ALD if a compound is dimerized under ALD conditions and dimers are less reactive. It could be subject of further studies to check whether the possibility interaction with surfaces exists for the non-chlorinated precursors.

3.8 Dimer opening

Finally, we tested the possibility of dimer opening reactions on the surface on the example of the $(\mathbf{3})_2$ dimer on SiO_2 . Fig. 9 shows the energy profile of the adsorption, dimer opening and subsequent dissociation of $(\mathbf{3})_2$.

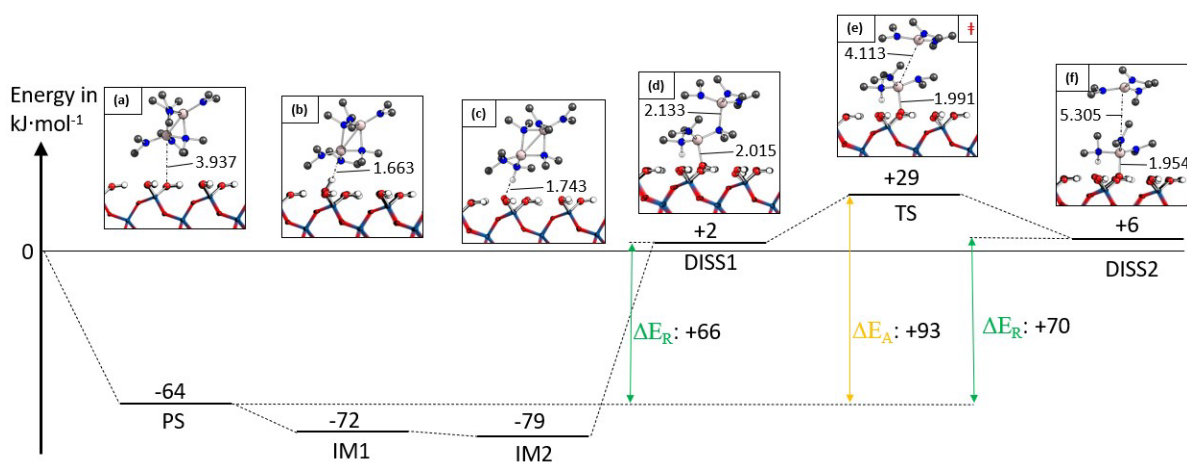


Figure 9. Reaction path of adsorption and dissociation of $(\mathbf{3})_2$ on SiO_2 . (a) Physisorbed dimer (PS) (b) First intermediary minimum (IM1) (c) Second intermediary minimum (IM2) (d) First partially dissociated structure (DISS1) (e) Transition state for the second dissociation step (TS) (f) Fully dissociated dimer (DISS2).

The reaction starts with the physisorbed state (PS) of the dimer and passes two intermediate minima (IM1 and IM2) where a proton is transferred to the dimethylamino-group until the dimer is opened and a chemical bond to the surface of 2.015 Å is formed (partially dissociated DISS1). The energy barriers of the proton transfer and that before the partially dissociated intermediary structure DISS1 are comparably small or negligible as it can be seen from the NEB-profile (see Fig. S6). Only the second dissociation step has a significant barrier and leads via the transition state (TS) to the final structure of the dissociated dimer (DISS2). The first dimer opening reaction is endothermic with $+66 \text{ kJ}\cdot\text{mol}^{-1}$ and the second dissociation step with $+70 \text{ kJ}\cdot\text{mol}^{-1}$. As a reference point for the reaction energy the PS structure was used. It also served as reference point

for the activation energy of $+93 \text{ kJ}\cdot\text{mol}^{-1}$ for the final dissociation because it can be assumed that the intermediary minima are passed quickly during the reaction.

The barrier height for the whole reaction is with $+93 \text{ kJ}\cdot\text{mol}^{-1}$ slightly below 1 eV ($96 \text{ kJ}\cdot\text{mol}^{-1}$). This is important because it is generally assumed that barriers above 1 eV are not overcome at ALD temperatures⁸⁶⁻⁸⁹. The barrier is also way lower compared to the dimerization energy of $+206 \text{ kJ}\cdot\text{mol}^{-1}$ for **(3)**₂ (see Tab. 2). This can in part be explained in chemical terms due to the transfer of a proton to the dimethylamino-group in the first step. The protonation withdraws electrons from the nitrogen and this electron withdrawing effect leads to an increased Lewis acidity on the neighboring aluminum, what makes the formation of a chemical bond to the surface oxygen with a free electron pair easier. The electron withdrawing effect furthermore polarizes the bond between N and Al in (d) what could also explain the relatively low barrier of $+27 \text{ kJ}\cdot\text{mol}^{-1}$ between (d) and (e) for the breaking of the second bond.

For the **(4)**₂ dimer, Kim et al.⁸⁴ calculated and discussed different reaction paths of dimer opening and decomposition reactions on the chemically similar Al_2O_3 surface in the study discussed before in section 3.5, using the MLP. Different to the reaction scheme in Fig. 9 where the dimer is opened and dissociates without further decomposition, they studied condensation reactions with the surface following the first breaking of the dimer bond. According to their result, the chemisorption and breaking of the first dimer bond (compare DISS1) is possible with a barrier below 1 eV with $71 \text{ kJ}\cdot\text{mol}^{-1}$ (0.74 eV), the subsequent reactions with the surface have higher activation energies with $131 \text{ kJ}\cdot\text{mol}^{-1}$ (1.36 eV) and $145 \text{ kJ}\cdot\text{mol}^{-1}$ (1.50 eV) depending on the condensation product. The energies to desorb the second fragment of **4** are even higher with $210 \text{ kJ}\cdot\text{mol}^{-1}$ (2.18 eV) and $214 \text{ kJ}\cdot\text{mol}^{-1}$ (2.22 eV) respectively. They also calculated similar condensation reactions of the monomer with the surface which had much lower barriers than those of the dimer. For one reaction pathway, the activation barriers were even below 1 eV. Therefore, the results by Kim et al.⁸⁴ indicate that only the monomer can undergo condensation reactions with the surface under ALD conditions. Consequently, a pathway of dimer opening and dissociation like in Fig. 9 followed by condensation reactions of these monomers with the surface would be a realistic way of how the **(4)**₂ dimer could react at the surface.

To further demonstrate the lower reactivity of the dimer, Kim et al.⁸⁴ have furthermore tested the adsorption of (4)₂ to Al₂O₃ between AlCH₃ fragments doubly bonded to the surface as SMIs and obtained a remarkably less stable structure compared to the free surface. Due to the higher effective size, dimers would have it more difficult to reach reactive groups between SMIs. And as the adsorption structures in 3.7 have shown, the dimers would not that easily adsorb to the surface or the inhibitor layer like monomers. The possibility of dimer opening on the surface does therefore by no means imply that dimerization has no effect on the reactivity of precursors and especially achieved selectivity in AS-ALD. It does however highlight the necessity to protect reactive surface groups during AS-ALD.

Conclusions

In this study the dimerization of a set of Al-precursors for ALD was calculated in dependence of pressure and temperature including conditions that are common for ALD. For the thermochemistry an improved approach including conformer search and DLPNO-CCSD(T) energies has been applied to obtain more accurate values than by DFT calculations alone. A comparison with typical DFT approaches has shown that the improved protocol gives results that can differ even qualitatively from DFT results when it comes to predictions of dimer dissociation. The calculated dimerization of the tested set of Al-precursors can be summarized as follows: TDMAA and DMAI are predicted to be present as dimers under all typical ALD conditions (pressures from 10^{-6} to 1 bar and temperatures from -50 to 400°C). In contrast, no relevant degree of dimerization is predicted for the aluminum-alkyls at the specific set of ALD conditions and the monomeric form remains preferred under variation of pressure or temperature. The precursors with branched alkyl chains show even a lower tendency to dimerization than the molecules with linear chains. The chlorinated precursors were at the transition between monomer and dimer, that means present in both forms under the above-mentioned conditions of $1.73 \cdot 10^{-4}$ bar (130 mTorr) and 200°C . This finding could open the possibility to influence the present form in ALD processes by choosing the right pressures and temperatures. To better understand the dimerization of precursors, bonding analyses on the bridging dimer bonds were performed. Energy decomposition analysis on the dimer bond shows that the preparation energy and Pauli repulsion are responsible for the weaker dimer bond of the aluminum alkyls than the chlorinated precursors. The relatively strong bond of TDMAA and DMAI is mainly explained by the electrostatic interaction.

Finally, the possible implications of dimerization on ALD chemistry were discussed. The adsorption of monomers compared to dimers on SiO_2 was tested and a weaker interaction of dimers with the surface was found, though the result depends on the precursor class. The possibility of dimer opening reactions on the surface exists, however, as the example of TDMAA dimer has shown. If precursors like TDMAA and DMAI are completely dimeric under ALD conditions, the dimer rather than the monomer needs to be considered when the precursor chemistry is discussed or investigated. In contrast, when the alkyl substituted Al-precursors are completely dissociated under ALD pressures and temperatures, dimerization does not play a role for any explanation of precursor reactivity. A field where the question of dimerization can be especially relevant are area

selective ALD applications. Here, the results on dimerization found in our study can help to explain the different reactivities of precursors like better performance of DMAI in AS-ALD processes than that of TMA. In understanding the impact of dimerization, calculations on dimer and monomer reactions and adsorption to the surface can be helpful in future studies.

Data availability statement

All computational data are available in the open access database Zenodo via DOI: 10.5281/zenodo.13325792.

Supporting Information. Further information on the accuracy of the computational approach, calculation of DDFs from thermodynamic considerations, more information on the EDA results and the NEB profile.

Acknowledgments

This work was supported by Merck KGaA via the 350th Anniversary Grant. We thank Prof. Stacey Bent and Alex Shearer for intense discussions and scientific exchange. We specifically thank Alex for the suggestion to include TiBA in this study. Computational resources were provided by ZIH Dresden, CSC-GOETHE Frankfurt, HLR Stuttgart and PC² Paderborn..

References

- (1) Oviroh, P. O.; Akbarzadeh, R.; Pan, D.; Coetzee, R. A. M.; Jen, T.-C. New Development of Atomic Layer Deposition: Processes, Methods and Applications. *Sci. Technol. Adv. Mater.* **2019**, *20* (1), 465–496. <https://doi.org/10.1080/14686996.2019.1599694>.
- (2) George, S. M. Atomic Layer Deposition: An Overview. *Chem. Rev.* **2010**, *110* (1), 111–131. <https://doi.org/10.1021/cr900056b>.
- (3) Mackus, A. J. M.; Merckx, M. J. M.; Kessels, W. M. M. From the Bottom-Up: Toward Area-Selective Atomic Layer Deposition with High Selectivity. *Chem. Mater.* **2019**, *31* (1), 2–12. <https://doi.org/10.1021/acs.chemmater.8b03454>.
- (4) O'Neill, B. J.; Jackson, D. H. K.; Lee, J.; Canlas, C.; Stair, P. C.; Marshall, C. L.; Elam, J. W.; Kuech, T. F.; Dumesic, J. A.; Huber, G. W. Catalyst Design with Atomic Layer Deposition. *ACS Catal.* **2015**, *5* (3), 1804–1825. <https://doi.org/10.1021/cs501862h>.
- (5) Gupta, B.; Hossain, Md. A.; Riaz, A.; Sharma, A.; Zhang, D.; Tan, H. H.; Jagadish, C.; Catchpole, K.; Hoex, B.; Karuturi, S. Recent Advances in Materials Design Using Atomic Layer Deposition for Energy Applications. *Adv. Funct. Mater.* **2022**, *32* (3), 2109105. <https://doi.org/10.1002/adfm.202109105>.
- (6) Foroughi-Abari, A.; Cadien, K. Atomic Layer Deposition for Nanotechnology. In *Nanofabrication*; Stepanova, M., Dew, S., Eds.; Springer Vienna: Vienna, 2012; pp 143–161. https://doi.org/10.1007/978-3-7091-0424-8_6.
- (7) Devi, A. 'Old Chemistries' for New Applications: Perspectives for Development of Precursors for MOCVD and ALD Applications. *Coord. Chem. Rev.* **2013**, *257* (23–24), 3332–3384. <https://doi.org/10.1016/j.ccr.2013.07.025>.
- (8) Hatanpää, T.; Ritala, M.; Leskelä, M. Precursors as Enablers of ALD Technology: Contributions from University of Helsinki. *Coord. Chem. Rev.* **2013**, *257* (23–24), 3297–3322. <https://doi.org/10.1016/j.ccr.2013.07.002>.
- (9) Oh, I.-K.; Sandoval, T. E.; Liu, T.-L.; Richey, N. E.; Nguyen, C. T.; Gu, B.; Lee, H.-B.-R.; Tonner-Zech, R.; Bent, S. F. Elucidating the Reaction Mechanism of Atomic Layer Deposition of Al₂O₃ with a Series of Al(CH₃)_xCl_{3-x} and Al(C_yH_{2y+1})₃ Precursors. *J. Am. Chem. Soc.* **2022**, *144* (26), 11757–11766. <https://doi.org/10.1021/jacs.2c03752>.

- (10) Potts, S. E.; Kessels, W. M. M. Energy-Enhanced Atomic Layer Deposition for More Process and Precursor Versatility. *Coord. Chem. Rev.* **2013**, *257* (23–24), 3254–3270. <https://doi.org/10.1016/j.ccr.2013.06.015>.
- (11) Leskelä, M.; Ritala, M. Atomic Layer Deposition (ALD): From Precursors to Thin Film Structures. *Thin Solid Films* **2002**, *409* (1), 138–146. [https://doi.org/10.1016/S0040-6090\(02\)00117-7](https://doi.org/10.1016/S0040-6090(02)00117-7).
- (12) Parsons, G. N.; Clark, R. D. Area-Selective Deposition: Fundamentals, Applications, and Future Outlook. *Chem. Mater.* **2020**, *32* (12), 4920–4953. <https://doi.org/10.1021/acs.chemmater.0c00722>.
- (13) Bonvalot, M.; Vallée, C.; Mannequin, C.; Jaffal, M.; Gassilloud, R.; Possémé, N.; Chevolleau, T. Area Selective Deposition Using Alternate Deposition and Etch Super-Cycle Strategies. *Dalton Trans.* **2022**, 442–450. <https://doi.org/10.1039/D1DT03456A>.
- (14) Oh, I.-K.; Sandoval, T. E.; Liu, T.-L.; Richey, N. E.; Bent, S. F. Role of Precursor Choice on Area-Selective Atomic Layer Deposition. *Chem. Mater.* **2021**, *33* (11), 3926–3935. <https://doi.org/10.1021/acs.chemmater.0c04718>.
- (15) Kim, H. G.; Kim, M.; Gu, B.; Khan, M. R.; Ko, B. G.; Yasmeen, S.; Kim, C. S.; Kwon, S.-H.; Kim, J.; Kwon, J.; Jin, K.; Cho, B.; Chun, J.-S.; Shong, B.; Lee, H.-B.-R. Effects of Al Precursors on Deposition Selectivity of Atomic Layer Deposition of Al₂O₃ Using Ethanethiol Inhibitor. *Chem. Mater.* **2020**, *32* (20), 8921–8929. <https://doi.org/10.1021/acs.chemmater.0c02798>.
- (16) Yarbrough, J.; Pieck, F.; Grigjanis, D.; Oh, I.-K.; Maue, P.; Tonner-Zech, R.; Bent, S. F. Tuning Molecular Inhibitors and Aluminum Precursors for the Area-Selective Atomic Layer Deposition of Al₂O₃. *Chem. Mater.* **2022**, *34* (10), 4646–4659. <https://doi.org/10.1021/acs.chemmater.2c00513>.
- (17) Merkx, M. J. M.; Angelidis, A.; Marnett, A.; Li, J.; Lemaire, P. C.; Sharma, K.; Hausmann, D. M.; Kessels, W. M. M.; Sandoval, T. E.; Mackus, A. J. M. Relation between Reactive Surface Sites and Precursor Choice for Area-Selective Atomic Layer Deposition Using Small Molecule Inhibitors. *J. Phys. Chem. C* **2022**, *126* (10), 4845–4853. <https://doi.org/10.1021/acs.jpcc.1c10816>.
- (18) Kim, H.; Kim, M.; Kim, B.; Shong, B. Adsorption Mechanism of Dimeric Ga Precursors in Metalorganic Chemical Vapor Deposition of Gallium Nitride. *J. Vac. Sci. Technol. A* **2023**, *41* (6), 063409. <https://doi.org/10.1116/6.0002966>.

- (19) Baev, A. K.; Shishko, M. A.; Korneev, N. N. Thermodynamics and Thermochemistry of Organoaluminum Compounds. *Russ. J. Gen. Chem.* **2002**, *72* (9), 1389–1395. <https://doi.org/10.1023/A:1021669611400>.
- (20) Laubengayer, A. W.; Gilliam, W. F. The Alkyls of the Third Group Elements. I. Vapor Phase Studies of the Alkyls of Aluminum, Gallium and Indium. *J. Am. Chem. Soc.* **1941**, *63* (2), 477–479. <https://doi.org/10.1021/ja01847a031>.
- (21) Smith, M. B. The Monomer–dimer Equilibria of Liquid Aluminum Alkyls. *J. Organomet. Chem.* **1972**, *46* (1), 31–49. [https://doi.org/10.1016/S0022-328X\(00\)90473-X](https://doi.org/10.1016/S0022-328X(00)90473-X).
- (22) Almenningen, A.; Halvorsen, S.; Haaland, A.; Pihlaja, K.; Schaumburg, K.; Ehrenberg, L. A Gas Phase Electron Diffraction Investigation of the Molecular Structures of Trimethylaluminium Monomer and Dimer. *Acta Chem. Scand.* **1971**, *25*, 1937–1945. <https://doi.org/10.3891/acta.chem.scand.25-1937>.
- (23) Lee, S. Y.; Luo, B.; Sun, Y.; White, J. M.; Kim, Y. Thermal Decomposition of Dimethylaluminum Isopropoxide on Si (1 0 0). *Appl. Surf. Sci.* **2004**, *222* (1–4), 234–242. <https://doi.org/10.1016/j.apsusc.2003.08.016>.
- (24) Champagne, B.; Mosley, D. H.; Fripiat, J. G.; Jean-Marie André; Bernard, A.; Bettonville, S.; François, P.; Momtaz, A. Dimerization versus Complexation of Triethylaluminum and Diethylaluminum Chloride: An Ab Initio Determination of Structures, Energies of Formation, and Vibrational Spectra. *J. Mol. Struct. THEOCHEM* **1998**, *454* (2–3), 149–159. [https://doi.org/10.1016/S0166-1280\(98\)00285-1](https://doi.org/10.1016/S0166-1280(98)00285-1).
- (25) Hay, J. N.; Hooper, P. G.; Robb, J. C. Monomer-Dimer Equilibria of Triethylaluminium. *J. Organomet. Chem.* **1971**, *28* (2), 193–204. [https://doi.org/10.1016/S0022-328X\(00\)84567-2](https://doi.org/10.1016/S0022-328X(00)84567-2).
- (26) Hiraoka, Y. S.; Mashita, M. Ab Initio Study on the Dimer Structures of Trimethylaluminum and Dimethylaluminumhydride. *J. Cryst. Growth* **1994**, *145* (1–4), 473–477. [https://doi.org/10.1016/0022-0248\(94\)91094-4](https://doi.org/10.1016/0022-0248(94)91094-4).
- (27) Wang, N. X.; Venkatesh, K.; Wilson, A. K. Behavior of Density Functionals with Respect to Basis Set. 3. Basis Set Superposition Error. *J. Phys. Chem. A* **2006**, *110* (2), 779–784. <https://doi.org/10.1021/jp0541664>.
- (28) Davidson, E. R.; Chakravorty, S. J. A Possible Definition of Basis Set Superposition Error. *Chem. Phys. Lett.* **1994**, *217* (1–2), 48–54. [https://doi.org/10.1016/0009-2614\(93\)E1356-L](https://doi.org/10.1016/0009-2614(93)E1356-L).

- (29) Ritala, M.; Leskelä, M.; Dekker, J.-P.; Mutsaers, C.; Soininen, P. J.; Skarp, J. Perfectly Conformal TiN and Al₂O₃ Films Deposited by Atomic Layer Deposition. *Chem. Vap. Depos.* **1999**, *5* (1), 7–9. [https://doi.org/10.1002/\(SICI\)1521-3862\(199901\)5:1<7::AID-CVDE7>3.0.CO;2-J](https://doi.org/10.1002/(SICI)1521-3862(199901)5:1<7::AID-CVDE7>3.0.CO;2-J).
- (30) Cremers, V.; Puurunen, R. L.; Dendooven, J. Conformality in Atomic Layer Deposition: Current Status Overview of Analysis and Modelling. *Appl. Phys. Rev.* **2019**, *6* (2), 021302. <https://doi.org/10.1063/1.5060967>.
- (31) Atkins, P. *Physikalische Chemie*, 2. Auflage.; VCH Verlagsgesellschaft GmbH: Weinheim, 1996.
- (32) Marques, E. A.; De Gendt, S.; Pourtois, G.; Van Setten, M. J. Benchmarking First-Principles Reaction Equilibrium Composition Prediction. *Molecules* **2023**, *28* (9), 3649. <https://doi.org/10.3390/molecules28093649>.
- (33) Buttera, S. C.; Mandia, D. J.; Barry, S. T. Tris(Dimethylamido)Aluminum(III): An Overlooked Atomic Layer Deposition Precursor. *J. Vac. Sci. Technol. Vac. Surf. Films* **2017**, *35* (1), 01B128. <https://doi.org/10.1116/1.4972469>.
- (34) Gladfelter, W. L. Selective Metalization by Chemical Vapor Deposition. *Chem. Mater.* **1993**, *5* (10), 1372–1388. <https://doi.org/10.1021/cm00034a004>.
- (35) Neese, F. The ORCA Program System. *WIREs Comput. Mol. Sci.* **2012**, *2* (1), 73–78. <https://doi.org/10.1002/wcms.81>.
- (36) Neese, F. Software Update: The ORCA Program System, Version 4.0. *WIREs Comput. Mol. Sci.* **2018**, *8* (1). <https://doi.org/10.1002/wcms.1327>.
- (37) Neese, F.; Wennmohs, F.; Becker, U.; Riplinger, C. The ORCA Quantum Chemistry Program Package. *J. Chem. Phys.* **2020**, *152* (22), 224108. <https://doi.org/10.1063/5.0004608>.
- (38) Grimme, S.; Antony, J.; Ehrlich, S.; Krieg, H. A Consistent and Accurate *Ab Initio* Parametrization of Density Functional Dispersion Correction (DFT-D) for the 94 Elements H-Pu. *J. Chem. Phys.* **2010**, *132* (15), 154104. <https://doi.org/10.1063/1.3382344>.
- (39) Grimme, S.; Ehrlich, S.; Goerigk, L. Effect of the Damping Function in Dispersion Corrected Density Functional Theory. *J. Comput. Chem.* **2011**, *32* (7), 1456–1465. <https://doi.org/10.1002/jcc.21759>.

- (40) Grimme, S. Accurate Description of van Der Waals Complexes by Density Functional Theory Including Empirical Corrections. *J. Comput. Chem.* **2004**, *25* (12), 1463–1473. <https://doi.org/10.1002/jcc.20078>.
- (41) Bykov, D.; Petrenko, T.; Izsák, R.; Kossmann, S.; Becker, U.; Valeev, E.; Neese, F. Efficient Implementation of the Analytic Second Derivatives of Hartree–Fock and Hybrid DFT Energies: A Detailed Analysis of Different Approximations. *Mol. Phys.* **2015**, *113* (13–14), 1961–1977. <https://doi.org/10.1080/00268976.2015.1025114>.
- (42) Riplinger, C.; Neese, F. An Efficient and near Linear Scaling Pair Natural Orbital Based Local Coupled Cluster Method. *J. Chem. Phys.* **2013**, *138* (3), 034106. <https://doi.org/10.1063/1.4773581>.
- (43) Pracht, P.; Bohle, F.; Grimme, S. Automated Exploration of the Low-Energy Chemical Space with Fast Quantum Chemical Methods. *Phys. Chem. Chem. Phys.* **2020**, *22* (14), 7169–7192. <https://doi.org/10.1039/C9CP06869D>.
- (44) Grimme, S. Exploration of Chemical Compound, Conformer, and Reaction Space with Meta-Dynamics Simulations Based on Tight-Binding Quantum Chemical Calculations. *J. Chem. Theory Comput.* **2019**, *15* (5), 2847–2862. <https://doi.org/10.1021/acs.jctc.9b00143>.
- (45) Becke, A. D. Density-Functional Exchange-Energy Approximation with Correct Asymptotic Behavior. *Phys. Rev. A* **1988**, *38* (6), 3098–3100. <https://doi.org/10.1103/PhysRevA.38.3098>.
- (46) Becke, A. D. Density-Functional Thermochemistry. III. The Role of Exact Exchange. *J. Chem. Phys.* **1993**, *98* (7), 5648–5652. <https://doi.org/10.1063/1.464913>.
- (47) Lee, C.; Yang, W.; Parr, R. G. Development of the Colle-Salvetti Correlation-Energy Formula into a Functional of the Electron Density. *Phys. Rev. B* **1988**, *37* (2), 785–789. <https://doi.org/10.1103/PhysRevB.37.785>.
- (48) Weigend, F.; Ahlrichs, R. Balanced Basis Sets of Split Valence, Triple Zeta Valence and Quadruple Zeta Valence Quality for H to Rn: Design and Assessment of Accuracy. *Phys. Chem. Chem. Phys.* **2005**, *7* (18), 3297. <https://doi.org/10.1039/b508541a>.
- (49) Weigend, F. Accurate Coulomb-Fitting Basis Sets for H to Rn. *Phys. Chem. Chem. Phys.* **2006**, *8* (9), 1057. <https://doi.org/10.1039/b515623h>.
- (50) Becke, A. D. A Multicenter Numerical Integration Scheme for Polyatomic Molecules. *J. Chem. Phys.* **1988**, *88* (4), 2547–2553. <https://doi.org/10.1063/1.454033>.

- (51) Liakos, D. G.; Neese, F. Is It Possible To Obtain Coupled Cluster Quality Energies at near Density Functional Theory Cost? Domain-Based Local Pair Natural Orbital Coupled Cluster vs Modern Density Functional Theory. *J. Chem. Theory Comput.* **2015**, *11* (9), 4054–4063. <https://doi.org/10.1021/acs.jctc.5b00359>.
- (52) Truhlar, D. G. Basis-Set Extrapolation. *Chem. Phys. Lett.* **1998**, *294* (1–3), 45–48. [https://doi.org/10.1016/S0009-2614\(98\)00866-5](https://doi.org/10.1016/S0009-2614(98)00866-5).
- (53) Dunning, T. H. Gaussian Basis Sets for Use in Correlated Molecular Calculations. I. The Atoms Boron through Neon and Hydrogen. *J. Chem. Phys.* **1989**, *90* (2), 1007–1023. <https://doi.org/10.1063/1.456153>.
- (54) Wedler, G.; Freund, H.-J. *Lehrbuch Der Physikalischen Chemie*, 6. Auflage.; WILEY-VCH: Weinheim, 2012.
- (55) Jensen, F. *Introduction to Computational Chemistry*, 1. Edition.; JOHN WILEY & SONS: Chichester, 1999.
- (56) Rüger, R.; Francini, M.; Trnka, T.; Yakovlev, A.; van Lenthe, E.; Philipsen, P.; van Vuren, T.; Klumpers, B.; Soini, T. AMS. <http://www.scm.com/> Accessed 3 July 2024.
- (57) Van Lenthe, E.; Baerends, E. J. Optimized Slater-type Basis Sets for the Elements 1–118. *J. Comput. Chem.* **2003**, *24* (9), 1142–1156. <https://doi.org/10.1002/jcc.10255>.
- (58) Chong, D. P.; Van Lenthe, E.; Van Gisbergen, S.; Baerends, E. J. Even-tempered Slater-type Orbitals Revisited: From Hydrogen to Krypton. *J. Comput. Chem.* **2004**, *25* (8), 1030–1036. <https://doi.org/10.1002/jcc.20030>.
- (59) Kitaura, K.; Morokuma, K. A New Energy Decomposition Scheme for Molecular Interactions within the Hartree-Fock Approximation. *Int. J. Quantum Chem.* **1976**, *10* (2), 325–340. <https://doi.org/10.1002/qua.560100211>.
- (60) Ziegler, T.; Rauk, A. Carbon Monoxide, Carbon Monosulfide, Molecular Nitrogen, Phosphorus Trifluoride, and Methyl Isocyanide as σ Donors and π Acceptors. A Theoretical Study by the Hartree-Fock-Slater Transition-State Method. *Inorg. Chem.* **1979**, *18* (7), 1755–1759. <https://doi.org/10.1021/ic50197a006>.
- (61) Ziegler, T.; Rauk, A. A Theoretical Study of the Ethylene-Metal Bond in Complexes between Cu^+ , Ag^+ , Au^+ , Pt^0 , or Pt^{2+} and Ethylene, Based on the Hartree-Fock-Slater Transition-State Method. *Inorg. Chem.* **1979**, *18* (6), 1558–1565. <https://doi.org/10.1021/ic50196a034>.

- (62) Bickelhaupt, F. M.; Nibbering, N. M. M.; Van Wezenbeek, E. M.; Baerends, E. J. Central Bond in the Three CN⁺ Dimers NC-CN, CN-CN and CN-NC: Electron Pair Bonding and Pauli Repulsion Effects. *J. Phys. Chem.* **1992**, *96* (12), 4864–4873. <https://doi.org/10.1021/j100191a027>.
- (63) Tonner, R.; Frenking, G. Divalent Carbon(0) Chemistry, Part 1: Parent Compounds. *Chem. – Eur. J.* **2008**, *14* (11), 3260–3272. <https://doi.org/10.1002/chem.200701390>.
- (64) Pecher, L.; Tonner, R. Deriving Bonding Concepts for Molecules, Surfaces, and Solids with Energy Decomposition Analysis for Extended Systems. *WIREs Comput. Mol. Sci.* **2019**, *9* (4), e1401. <https://doi.org/10.1002/wcms.1401>.
- (65) Bickelhaupt, F. M.; Baerends, E. J. Kohn-Sham Density Functional Theory: Predicting and Understanding Chemistry. In *Reviews in Computational Chemistry*; Lipkowitz, K. B., Boyd, D. B., Eds.; Wiley, 2000; Vol. 15, pp 1–86. <https://doi.org/10.1002/9780470125922.ch1>.
- (66) Te Velde, G.; Bickelhaupt, F. M.; Baerends, E. J.; Fonseca Guerra, C.; Van Gisbergen, S. J. A.; Snijders, J. G.; Ziegler, T. Chemistry with ADF. *J. Comput. Chem.* **2001**, *22* (9), 931–967. <https://doi.org/10.1002/jcc.1056>.
- (67) Kresse, G.; Hafner, J. *Ab Initio* Molecular Dynamics for Liquid Metals. *Phys. Rev. B* **1993**, *47* (1), 558–561. <https://doi.org/10.1103/PhysRevB.47.558>.
- (68) Kresse, G.; Hafner, J. *Ab Initio* Molecular-Dynamics Simulation of the Liquid-Metal–Amorphous-Semiconductor Transition in Germanium. *Phys. Rev. B* **1994**, *49* (20), 14251–14269. <https://doi.org/10.1103/PhysRevB.49.14251>.
- (69) Kresse, G.; Furthmüller, J. Efficiency of *Ab-Initio* Total Energy Calculations for Metals and Semiconductors Using a Plane-Wave Basis Set. *Comput. Mater. Sci.* **1996**, *6* (1), 15–50. [https://doi.org/10.1016/0927-0256\(96\)00008-0](https://doi.org/10.1016/0927-0256(96)00008-0).
- (70) Kresse, G.; Furthmüller, J. Efficient Iterative Schemes for *Ab Initio* Total-Energy Calculations Using a Plane-Wave Basis Set. *Phys. Rev. B* **1996**, *54* (16), 11169–11186. <https://doi.org/10.1103/PhysRevB.54.11169>.
- (71) Kresse, G.; Hafner, J. Norm-Conserving and Ultrasoft Pseudopotentials for First-Row and Transition Elements. *J. Phys. Condens. Matter* **1994**, *6* (40), 8245–8257. <https://doi.org/10.1088/0953-8984/6/40/015>.
- (72) Perdew, J. P.; Burke, K.; Ernzerhof, M. Generalized Gradient Approximation Made Simple. *Phys. Rev. Lett.* **1996**, *77* (18), 3865–3868. <https://doi.org/10.1103/PhysRevLett.77.3865>.

- (73) Kresse, G.; Joubert, D. From Ultrasoft Pseudopotentials to the Projector Augmented-Wave Method. *Phys. Rev. B* **1999**, *59* (3), 1758–1775. <https://doi.org/10.1103/PhysRevB.59.1758>.
- (74) Monkhorst, H. J.; Pack, J. D. Special Points for Brillouin-Zone Integrations. *Phys. Rev. B* **1976**, *13* (12), 5188–5192. <https://doi.org/10.1103/PhysRevB.13.5188>.
- (75) Pack, J. D.; Monkhorst, H. J. “Special Points for Brillouin-Zone Integrations”—a Reply. *Phys. Rev. B* **1977**, *16* (4), 1748–1749. <https://doi.org/10.1103/PhysRevB.16.1748>.
- (76) Momma, K.; Izumi, F. *VESTA 3* for Three-Dimensional Visualization of Crystal, Volumetric and Morphology Data. *J. Appl. Crystallogr.* **2011**, *44* (6), 1272–1276. <https://doi.org/10.1107/S0021889811038970>.
- (77) Gražulis, S.; Chateigner, D.; Downs, R. T.; Yokochi, A. F. T.; Quirós, M.; Lutterotti, L.; Manakova, E.; Butkus, J.; Moeck, P.; Le Bail, A. Crystallography Open Database – an Open-Access Collection of Crystal Structures. *J. Appl. Crystallogr.* **2009**, *42* (4), 726–729. <https://doi.org/10.1107/S0021889809016690>.
- (78) Kroll, P.; Milko, M. Theoretical Investigation of the Solid State Reaction of Silicon Nitride and Silicon Dioxide Forming Silicon Oxynitride (Si₂N₂O) under Pressure. *Z. Für Anorg. Allg. Chem.* **2003**, *629* (10), 1737–1750. <https://doi.org/10.1002/zaac.200300122>.
- (79) Henkelman, G.; Jónsson, H. Improved Tangent Estimate in the Nudged Elastic Band Method for Finding Minimum Energy Paths and Saddle Points. *J. Chem. Phys.* **2000**, *113* (22), 9978–9985. <https://doi.org/10.1063/1.1323224>.
- (80) Henkelman, G.; Uberuaga, B. P.; Jónsson, H. A Climbing Image Nudged Elastic Band Method for Finding Saddle Points and Minimum Energy Paths. *J. Chem. Phys.* **2000**, *113* (22), 9901–9904. <https://doi.org/10.1063/1.1329672>.
- (81) Sheppard, D.; Terrell, R.; Henkelman, G. Optimization Methods for Finding Minimum Energy Paths. *J. Chem. Phys.* **2008**, *128* (13), 134106. <https://doi.org/10.1063/1.2841941>.
- (82) Smidstrup, S.; Pedersen, A.; Stokbro, K.; Jónsson, H. Improved Initial Guess for Minimum Energy Path Calculations. *J. Chem. Phys.* **2014**, *140* (21), 214106. <https://doi.org/10.1063/1.4878664>.
- (83) Hackler, R. A.; McAnally, M. O.; Schatz, G. C.; Stair, P. C.; Van Duyne, R. P. Identification of Dimeric Methylalumina Surface Species during Atomic Layer Deposition Using *Operando* Surface-Enhanced Raman Spectroscopy. *J. Am. Chem. Soc.* **2017**, *139* (6), 2456–2463. <https://doi.org/10.1021/jacs.6b12709>.

- (84) Kim, M.; Kim, S.; Shong, B. Adsorption of Dimethylaluminum Isopropoxide (DMAI) on the Al₂O₃ Surface: A Machine-Learning Potential Study. *J. Sci. Adv. Mater. Devices* **2024**, 100754. <https://doi.org/10.1016/j.jsamd.2024.100754>.
- (85) Seo, S.; Yeo, B. C.; Han, S. S.; Yoon, C. M.; Yang, J. Y.; Yoon, J.; Yoo, C.; Kim, H.; Lee, Y.; Lee, S. J.; Myoung, J.-M.; Lee, H.-B.-R.; Kim, W.-H.; Oh, I.-K.; Kim, H. Reaction Mechanism of Area-Selective Atomic Layer Deposition for Al₂O₃ Nanopatterns. *ACS Appl. Mater. Interfaces* **2017**, 9 (47), 41607–41617. <https://doi.org/10.1021/acsami.7b13365>.
- (86) Yu, P.; Merx, M. J. M.; Tezsevin, I.; Lemaire, P. C.; Hausmann, D. M.; Sandoval, T. E.; Kessels, W. M. M.; Mackus, A. J. M. Blocking Mechanisms in Area-Selective ALD by Small Molecule Inhibitors of Different Sizes: Steric Shielding versus Chemical Passivation. *Appl. Surf. Sci.* **2024**, 665, 160141. <https://doi.org/10.1016/j.apsusc.2024.160141>.
- (87) Ande, C. K.; Elliott, S. D.; Kessels, W. M. M. First-Principles Investigation of C–H Bond Scission and Formation Reactions in Ethane, Ethene, and Ethyne Adsorbed on Ru(0001). *J. Phys. Chem. C* **2014**, 118 (46), 26683–26694. <https://doi.org/10.1021/jp5069363>.
- (88) Shirazi, M.; Elliott, S. D. Cooperation between Adsorbates Accounts for the Activation of Atomic Layer Deposition Reactions. *Nanoscale* **2015**, 7 (14), 6311–6318. <https://doi.org/10.1039/C5NR00900F>.
- (89) Shirazi, M.; Elliott, S. D. Multiple Proton Diffusion and Film Densification in Atomic Layer Deposition Modeled by Density Functional Theory. *Chem. Mater.* **2013**, 25 (6), 878–889. <https://doi.org/10.1021/cm303630e>.